JOURNAL OF GEOPHYSICAL RESEARCH: EARTH SURFACE, VOL. 118, 1806–1825, doi:10.1002/jgrf.20113, 2013

Lithologic and tectonic controls on bedrock channel form at the northwest Himalayan front

George H. Allen,[1] Jason B. Barnes,[1] Tamlin M. Pavelsky,[1] and Eric Kirby[2,3]

Received 17 September 2012; revised 8 July 2013; accepted 11 July 2013; published 12 September 2013.

[1] Recognition that channel form reflects a river's ability to erode rock and transport material has spawned stream-power models that estimate incision patterns by approximating energy dissipation within a channel. These models frequently assume that channel width scales as a power law with drainage area, partly because drainage area is easily extracted from digital elevation models (DEMs). However, this assumption is often confounded by local variations in rock strength and rock-uplift rate that can cause channel constriction downstream. Here we investigate the morphological response to spatial changes in rock strength and rock-uplift rate of 10 bedrock channels traversing the Mohand range along the northwest Himalayan front. We present a new method to continuously measure and compare channel width, slope, and other hydraulic parameters that integrate satellite imagery and DEM analysis. Our method corrects for an ~13% overestimation of average channel gradient from a 90 m resolution DEM that arises from short circuits of fine-scale meanders. We find that channels (1) narrow >1 km upstream from knickpoints formed by an increase in rock strength, (2) adjust laterally more than vertically in response to downstream decreases rock erodibility and uplift rate, and (3) meander where shear stresses are high and channel widths are low. We attribute these results to a high ratio of sediment supply to transport capacity, which enhances lateral erosion relative to vertical incision. Our results suggest that substrate strength and sediment supply substantially influence channel form and that channel width should be explicitly measured when interpreting tectonic signals from bedrock channel morphology.

Citation: Allen, G. H., J. B. Barnes, T. M. Pavelsky, and E. Kirby (2013), Lithologic and tectonic controls on bedrock channel form at the northwest Himalayan front, *J. Geophys. Res. Earth Surf.*, *118*, 1806–1825, doi:10.1002/jgrf.20113.

1. Introduction

[2] Bedrock rivers set the long-term denudation rates of mountain belts by setting base level for hillslope processes, incising into rock, and transporting material out to the lowlands [*Burbank et al*., 1996; *Howard et al*., 1994; *Molnar and England*, 1990]. They dictate the first-order response of mountain ranges to external forcing by communicating tectonic and climatic signals across the landscape through adjustment of their channel form (see review by *Kirby and Whipple* [2012]). Given this connection between bedrock channel form and forcing, recent studies suggest that tectonic and climatic information can be extracted from patterns of bedrock channel geometry [e.g., *Gallen et al*., 2013; *Stark et al*., 2010]. Hillslope gradient and relief have also been proposed as important metrics for erosion, but thresholds in transport processes lead to limited adjustment beyond relatively low erosion rates [*Montgomery and Brandon*, 2002; *Ouimet et al*., 2009]. These observations suggest that bedrock rivers are perhaps the geomorphic landscape feature that best encodes signals of tectonic and climatic forcing in highlands [*Whittaker*, 2012]. Unfortunately, establishing the link between a particular forcing and channel form is often challenging because the latter may reflect adjustment to other factors including substrate erodibility, sediment supply, hydraulic roughness, vegetation, and hillslope processes that vary in space and time [*Duvall et al*., 2004; *Finnegan et al*., 2007; *Goode and Wohl*, 2010; *Montgomery et al*., 1996; *Walsh et al*., 2012; *Whittaker et al*., 2008].

[3] Channel slope and width reflect river erosional capacity because rivers with steep, narrow channels flow faster over a smaller cross-sectional area, focusing more energy on the bed and increasing sediment transport and erosion. Stream-power models use channel form to estimate patterns of bedrock incision by approximating energy dissipation within a channel [*Finnegan et al*., 2005; *Howard*, 1994; *Howard and Kerby*, 1983; *Whipple and Tucker*, 1999]. These models most commonly focus on changes in channel slope because slope controls the rate of potential energy expenditure per unit of downstream distance and because channel width is

[1]Department of Geological Sciences, University of North Carolina at Chapel Hill, Chapel Hill, North Carolina, USA.
[2]Department of Geosciences, Pennsylvania State University, University Park, Pennsylvania, USA.
[3]Now at College of Earth, Ocean and Atmospheric Sciences, Oregon State University, Corvallis, Oregon, USA.

Corresponding author: G. H. Allen, Department of Geological Sciences, University of North Carolina at Chapel Hill, 104 South Road, Mitchell Hall, Campus Box #3315, Chapel Hill, NC 27599-3315, USA. (geoallen@unc.edu)

2169-9003/13/10.1002/jgrf.20113

difficult to accurately extract from a DEM or measure in rugged terrain [*Wobus et al*., 2008]. However, lateral adjustments in channel form may be equally important because width represents another way that channels can respond to changing boundary conditions [*Stark*, 2006; *Stark et al*., 2010; *Turowski et al*., 2007; *Turowski et al*., 2008; *Wobus et al*., 2006b; *Yanites and Tucker*, 2010; *Yanites et al*., 2010].

[4] Observing channel gradient alone may not fully capture channel adjustment to external forcing because rivers adjust their slopes and widths differently to variations in lithology [*Montgomery and Gran*, 2001] or rock-uplift rate [*Amos and Burbank*, 2007; *Yanites et al*., 2010]. Field-based studies have used measurements to empirically estimate channel width variations in the context of stream-power models [*Anderson*, 1994; *Duvall et al*., 2004; *Finnegan et al*., 2005; *Harbor*, 1998; *Lavé and Avouac*, 2000, 2001; *Snyder et al*., 2003a; *Stock and Montgomery*, 1999; *Tomkin et al*., 2003; *Whittaker et al*., 2007; *Yanites et al*., 2010]. In most of these studies, channel width was measured by hand either from satellite images or in the field, thus subsampling at a relatively coarse resolution (e.g., every 100 m in *Finnegan et al*. [2005]), and potentially biasing the data. Continuous measurement of both vertical and lateral channel geometry components may yield new insights into the processes of channel adjustment to external forcing. Further, regional-scale stream-power studies often consider only first-order changes in rock erodibility, overlooking smaller-scale yet potentially important stratigraphic controls on channel adjustment.

[5] In steady state landscapes, rivers balance downstream increases in rock strength and rock-uplift rate by adjusting their channel geometry to generate increased stream power for a given discharge [*Whipple and Tucker*, 1999]. An increase in stream power causes the flow to exceed a critical threshold necessary to transport sediment for a greater proportion of time [*Gilbert*, 1877; *Sklar and Dietrich*, 1998]. If sediment supply is high relative to transport capacity, material deposited on the channel bed inhibits vertical incision, promotes lateral erosion, and forms a wide, shallow channel [*Finnegan et al*., 2007; *Turowski et al*., 2007]. Thus, given adequate sediment supply and equilibrium conditions, downstream variations in rock strength and/or rock-uplift rate will cause rivers to modify their incision potential by adjusting their widths and not necessarily only their slopes. Following previous studies, we hypothesize that where rock strength and/or uplift rate decreases downstream, channel width adjustments may become decoupled from changes in drainage area and/or slope [*Turowski et al*., 2007; *Yanites and Tucker*, 2010]. We test these ideas by applying a new method that integrates satellite image and digital topographic analysis to estimate bedrock channel width and slope continuously downstream along channels traversing the Mohand range at the northwest Himalayan front in India [*Thakur*, 1995]. The Mohand range is a natural laboratory for exploring channel adjustment to changes in rock erodibility and rock-uplift rate because these factors vary systemically across the region.

2. Downstream Hydraulic Scaling

[6] In theory, if tectonic and climatic conditions do not vary over long periods of time (>100 kyr in most settings), bedrock channels converge toward an equilibrium form whereby incision balances rock uplift [*Whipple*, 2004]. If other factors that affect channel morphology (e.g., substrate erodibility, precipitation gradients, sediment supply, and grain size distribution) remain uniform, channels exhibit well-documented hydraulic scaling relationships similar to those observed in self-formed alluvial rivers [e.g., *Wohl*, 2004; *Wohl and David*, 2008]. Hydraulic scaling relates longitudinal and cross-sectional channel geometry to discharge and/or drainage area with theoretically and empirically derived power law functions [*Hack*, 1957; *Leopold and Maddock*, 1953]. In particular, downstream changes in channel slope and width relative to upstream drainage area have been well studied partly because this information can be used to estimate the incision and sediment transport capacity of a stream [*Bagnold*, 1980; *Howard and Kerby*, 1983].

2.1. Channel Slope

[7] Channel slope regulates the rate at which potential energy is lost per unit downstream distance and is often considered the most important hydraulic parameter for estimating incision [e.g., *Howard and Kerby*, 1983; *Lavé and Avouac*, 2001]. Channels frequently display a graded profile described by a power law relationship between local slope (S) and contributing upstream drainage area (A):

$$S = k_s A^{-\theta}, \tag{1}$$

where k_s is the steepness index and θ is the concavity index (Figures 1a and 1b) [*Flint*, 1974]. The concavity index is determined by fitting a power law relationship to slope-area data from the equilibrium channel reaches (i.e., those without knickpoints, rock-uplift rate gradients, or changes in substrate downstream) (Figure 1c) [*Wobus et al*., 2006a]. To compare steepness across channel segments with varying drainage areas and concavity indices, a regional mean concavity index is determined and used as a reference (θ_{ref}), allowing for the empirical calculation of the normalized steepness index,

$$k_{sn} = SA^{\theta_{ref}}, \tag{2}$$

a measure of relative steepness (Figure 1d) [*Wobus et al*., 2006a]. Normalized steepness is a useful metric because it can be calculated by automated information extraction from digital elevation models (DEMs) and has been shown to correlate with erosion rate [e.g., *Cyr et al*., 2010; *Ouimet et al*., 2009; *Safran et al*., 2005; see also review by *Kirby and Whipple*, 2012].

2.2. Channel Width

[8] Channel width determines the quantity of energy exerted on a channel's bed per unit area, with a reduction in width focusing this energy and enhancing incision.

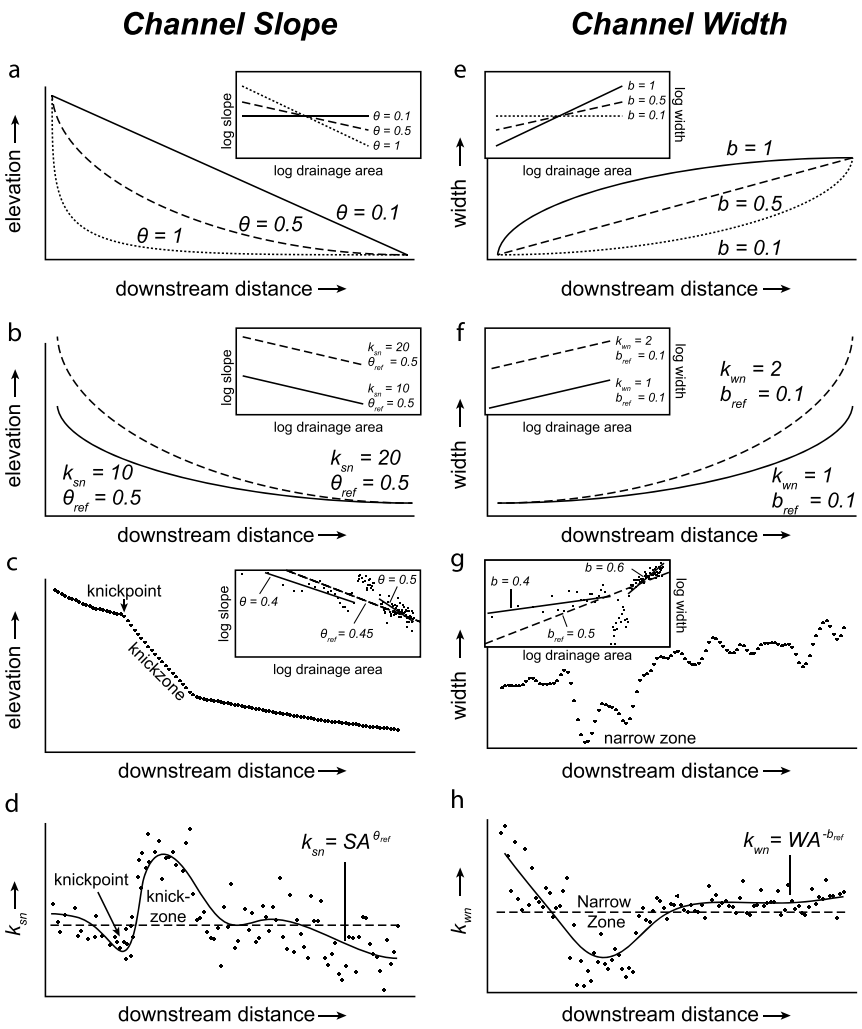

Figure 1. Idealized variations in channel form parameters downstream. Equilibrium long profiles with varying concavity indices (a) and steepness indices (b) with insets displaying slope-area data [modified after *Duvall et al*., 2004; *Whipple and Tucker*, 1999]. (c) Long profile with a knickpoint and knickzone. Inset shows reference concavity (dashed line slope) set by linear regressions through the equilibrium slope-area reaches (solid lines). (d) Long profile of raw (dots) and smoothed (line) normalized steepness index (k_{sn}) from the profile in Figure 1c. Dashed horizontal line is mean k_{sn} and equivalent to θ_{ref} (inset of part c). (e) Equilibrium channel width long profiles with varying width exponents assuming a square increase in drainage area with increasing distance downstream. Inset is the width-area data. (f) Equilibrium long width profiles with varying wideness indices (k_{wn}) and fixed width exponent b. Inset shows same profiles in width-area space. (g) Idealized width long profile with an intermediate narrow zone. Inset shows reference width exponent (dashed line slope) determined by linear regressions through equilibrium width-area reaches (solid lines). (h) Long profile of raw (dots) and smoothed (line) normalized wideness index (k_{wn}). Dashed horizontal line is average k_{wn} and equivalent to b_{ref} (inset of Figure 1g).

Channels often exhibit power law scaling between width (W) and upstream drainage area:

$$W = k_w A^b, \tag{3}$$

where k_w is the width coefficient and b is the width exponent ($b \cong 0.3$ - 0.5) (Figures 1e and 1f) [*Hack*, 1957; *Whipple*, 2004]. The width coefficient is an empirical parameter of channel geometry, but it can also be directly related to incision potential based on stream-power models. By combining incision models that assume steady state equilibrium and power law scaling of slope with drainage area, the width coefficient, hereafter referred to as the wideness index, can be considered a metric for the degree to which channel width adjusts in response to forcing. Similar to θ_{ref} in equation (2), a mean width exponent can be determined for equilibrium channel reaches, yielding a reference wideness exponent (b_{ref}) (Figure 1g). Applying b_{ref} to width-area data produces the normalized wideness index,

$$k_{wn} = WA^{-b_{ref}}, \tag{4}$$

a parameter that allows for quantitative comparison of channel widths across a region (Figure 1h). See Appendix A

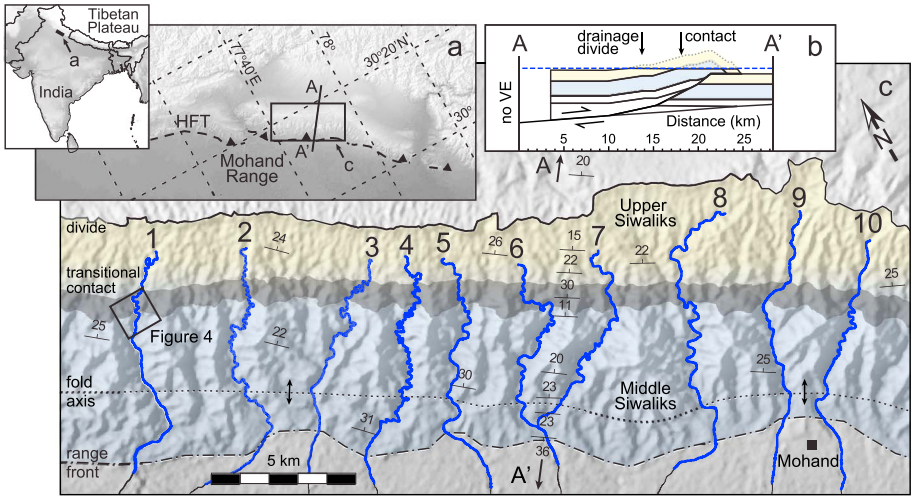

Figure 2. The Mohand range in the Siwalik Hills, northwest India. (a) The topography results from hanging wall uplift above a Himalayan Frontal Thrust (HFT) segment (fault from *Raiverman et al.* [1990]). (b) Balanced cross section through the central Mohand (location in Figure 2c) [simplified from *Barnes et al.*, 2011; *Mishra and Mukhopadhyay*, 2002]. Blue dashed line is the mean channel elevation. (c) The 10-studied channels flowing southwestward across the central portion of the range. Channels begin in Upper Siwaliks conglomerates (yellow), cross a transitional contact (dark gray), and then traverse Middle Siwaliks sandstones (blue-gray) before entering the foreland. South of the fold axis (dotted line), channels cross a zone of little rock uplift above a flat within the HFT near the range front. Contacts from field mapping and fold axis from *Mishra and Mukhopadhyay* [2002] and *Thakur et al.* [2007].

for the full derivation of the wideness index. We consider downstream variations in k_{wn}, conceptually equivalent to k_{sn}, to be an empirical measure of the deviation from a regional equilibrium width-area scaling set by b_{ref}.

3. Geologic and Geomorphic Setting

[9] Nearly half of the Quaternary convergence between India and Asia (~40 mm/yr) has been focused near the Himalayan front [*Bilham et al.*, 1997; *England and Molnar*, 1997; *Kumar et al.*, 2001]. Much of this convergence is accommodated along the Himalayan Frontal Thrust (HFT) [*Lavé and Avouac*, 2001; *Wesnousky et al.*, 1999]. The HFT is a segmented, blind-to-emergent fault recognized as the main tectonic and topographic boundary (or discontinuity) between the Himalayas and the Gangetic foreland basin (Figure 2) [*Kumar et al.*, 2006; *Nakata*, 1989; *Thakur*, 2013]. Shortening along the HFT drives uplift of the Siwalik Hills, foothill ranges that are composed of poorly lithified Miocene-Pliocene foreland basin sediments of the Siwalik Group [*Malik and Nakata*, 2003; *Yeats and Lillie*, 1991; *Yeats and Thakur*, 2008].

[10] Bedrock rivers draining the Siwalik Hills are likely in or near steady state equilibrium with the active faulting because (1) patterns in river incision potential match rock-uplift rates inferred from dated fluvial terraces [*Lavé and Avouac*, 2000, 2001], (2) channels exhibit well-graded elevation profiles where rock types and uplift do not vary [*Kirby and Whipple*, 2001], and (3) a combination of weak uplifting rock and high discharge during monsoons facilitate erosionally efficient river and overland flow that keeps hillslopes near failure and allows channels to rapidly adjust to the active deformation [*Barnes et al.*, 2011].

[11] In northwestern India, the Mohand range is a Siwalik uplift structure that is ~80 km long by ~15 km wide with ~500 m of total relief (Figure 2) [*Rao et al.*, 1975]. Geologic and geophysical data indicate the Mohand is a fault-bend fold in the HFT hanging wall [*Kumar et al.*, 2006; *Powers et al.*, 1998; *Wesnousky et al.*, 1999]. In the central portion of the fold, the HFT has slipped ~4–5 km along a variably dipping (~30°–20°NE) ramp that changes into a flat close to the southwestern mountain front near the fold axis (Figures 2b and 2c) [*Mishra and Mukhopadhyay*, 2002; *Powers et al.*, 1998]. As a consequence of this fault geometry, average rock-uplift rates between the range flanks vary [*Barnes et al.*, 2011] but are likely relatively uniform and high across most of the southern flank [*Kirby and Whipple*, 2012]. The exception occurs near the southern range front where the HFT ramp changes to a flat resulting in a zone of little to no rock uplift. Regional magnetostratigraphy data from the Siwaliks rocks suggest that deformation began less than ~0.8 Ma [*Sangode and Kumar*, 2003]. Near the town of Mohand (Figure 2c), a radiocarbon dated fluvial terrace suggests a HFT slip rate of $\geq 13.8 \pm 3.16$ mm/yr and a rock-uplift rate of 6.9 ± 1.8 mm/a [*Wesnousky et al.*, 1999], consistent with the total displacement and duration. Erosion plays a dominant role in shaping the Mohand range topography as suggested by a drainage divide recessed toward the hinterland relative to the fold axis (Figure 2c) [*Gupta and Ellis*, 2004] and removal of an estimated ~85% of the total uplifted rock since faulting began [*Barnes et al.*, 2011].

[12] A linear range front and ample bedrock exposure suggest that the first-order geologic structure does not vary along strike within a central portion of the Mohand (Figure 2) [*Barnes et al.*, 2011]. In this study area, bedrock rivers flow southwest from the divide, traversing down section

Figure 3. Field photos of the Siwaliks stratigraphy and channel-to-hillslope scale geomorphology in the Mohand range. Upper Siwaliks conglomerates have (a) cobble-sized clasts within a poorly lithified sandstone matrix and (b) wide channels with low banks and moderate hillslope relief. (c) Middle Siwaliks contain multistory cross-bedded sandstones (person for scale), and (d) narrow channels with steep banks and high hillslope relief (person for scale).

through Mio-Pleistocene Upper Siwaliks, across a transitional contact, and then across older Middle Siwaliks before reaching the open foreland basin (Figure 2c) [*Kumar and Nanda*, 1989; *Kumar and Ghosh*, 1991]. The Upper Siwaliks are thick beds of quartzite-cobble conglomerates with a sand matrix and the Middle Siwaliks are poorly indurated multistory sandstones (Figures 3a and 3c) [*Kumar*, 1993].

[13] The Mohand channels have bedrock banks and their beds are covered by sand to cobble-sized sediment with occasional bedrock exposures suggesting high sediment supply relative to transport capacity (Figures 3b and 3d). Channels occupy most, if not all, of the valley floor and possess steep cut banks and gentler slopes on the inside of meander bends. Bed load size is limited by the cobble-sized clasts sourced from the Upper Siwaliks conglomerates. The abundant sediment appears to break down into a bimodal size distribution (sand and cobbles) throughout the channels very quickly (Figure 3). The sediment is predominantly transported downstream during monsoon-driven flood events that account for ~80% of the ~1–2 m/yr mean annual precipitation within the study area [*Bookhagen and Burbank*, 2006; 2010; *Mohindra et al*., 1992]. As a result, channels contain ephemeral rivers characterized by high discharges implying efficient but episodic sediment transport and incision [*Barnes et al*., 2011] and have a typical hydraulic roughness that varies little except where isolated patches of bedrock are exposed.

4. Methods

4.1. Field Data

[14] We investigated the central Mohand geology and measured proxies for rock erodibility and channel morphology in selected areas in winter 2011. We augmented existing stratigraphic sections [*Kumar*, 1993; *Kumar and Nanda*, 1989] with our own field observations of the nature and location of the transition from Upper-to-Middle Siwaliks along five channels in the area (channels 1, 3, 4, 8, and 9 in Figure 2c). We then interpolated between these locations using the intersection between topography and contact surfaces projected parallel to the average rock orientation.

[15] Rock erodibility exerts a first-order control on channel morphology and incision [*Montgomery and Gran*, 2001; *Sklar and Dietrich*, 2001; *Sklar and Dietrich*, 2004; *Whipple*, 2004; *Whipple et al*., 2000]. Intact rock strength and fracture spacing are thought to govern bedrock erodibility [e.g., *Hack*, 1957; *Selby*, 1993; *Stock and Montgomery*, 1999]. We quantified intact rock strength using a type N Schmidt Hammer, a spring-loaded device that measures rebound values that scale with unconfined rock strength estimates made in laboratory tests [*Cargill and Shakoor*, 1990; *Selby*, 1993]. We estimated intact rock strength at 10 sites in the Upper Siwaliks and 13 in the Middle Siwaliks by recording 40 rebound measurements per site and discarding all measurements below a rebound value of 11 [after *Duvall et al*., 2004; *Snyder et al*., 2003a]. In the Upper Siwaliks, we restricted our

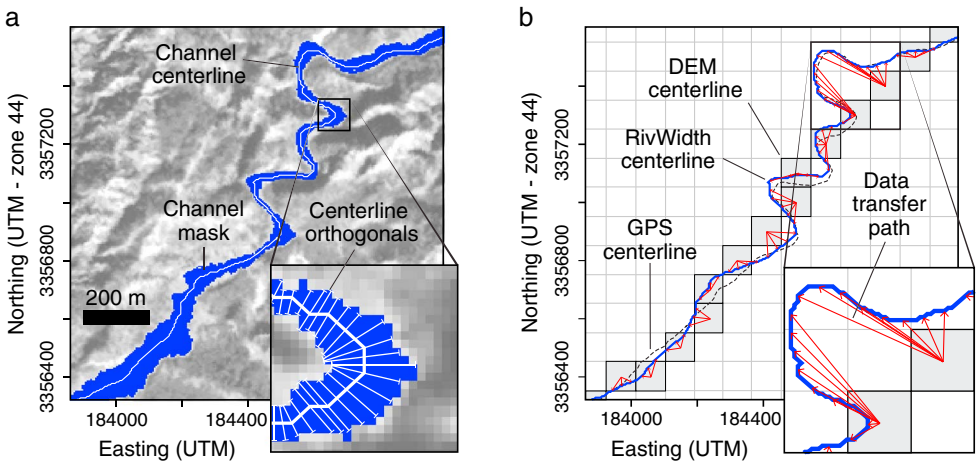

Figure 4. Methods for measuring channel form (location in Figure 2c). (a) 5 m resolution SPOT 5 image overlain by RivWidth channel mask (blue) and centerline (white). Inset is channel width (white bars) measured perpendicular to the centerline at each pixel. (b) DEM channel pixels (gray) overlain by channel centerlines determined with RivWidth (blue) and differential GPS (black dashes) for comparison. Red arrows, enlarged in inset, shows how the DEM-derived information (elevation, drainage area) is transferred to the nearest equivalent pixel in the image-based channel centerline with the relevant width value. This transfer process assigns multiple-image-based centerline pixels the same elevation value, thus elongating the DEM-derived long profile.

measurements to the conglomerate matrix because it is the weakest component and thus sets the bedrock strength limit. We also estimated intact rock strength with "simple means" field testing because the type N Schmidt Hammer is not designed for weak lithologies [*Goudie*, 2006]. The simple means test is a semiquantitative method used primarily in the geomechanics field that classifies a rock's response to hand compression and hammer blows. Results have been shown to complement and be consistent with Schmidt Hammer measurements for approximating rock strength [*Hack and Huisman*, 2002]. We conducted 20 simple means testing measurements at the same sites as the Schmidt Hammer measurements. We compared the mean values of each location and combined them into a single average and standard deviation for each Siwaliks unit using the Schmidt Hammer and simple means data separately.

[16] Bedrock erodibility is also affected by fractures because they increase the efficiency of hydraulic plucking and promote bedrock weathering by increasing surface area exposure [*Clarke and Burbank*, 2011; *Hancock et al.*, 2011]. We measured fracture spacing at the same sites we took intact rock strength measurements, choosing locations that were representative of the entire outcrop exposed. At each site, we used three 1 m scan lines over which we measured fracture spacing perpendicular to bedding, parallel to strike, and parallel to dip [after *Dühnforth et al.*, 2010; *Gillespie et al.*, 1993].

[17] We also measured channel form along selected reaches in the field to validate our remote-sensing-based estimates because our method is novel and needed testing. We quantified bankfull width at 40 different locations using a handheld laser range finder and compared these field-based widths to the nearest channel width estimated from the satellite image. We also measured channel slope with a continuous differential GPS along several channel reaches.

4.2. Remote Sensing

[18] We quantified channel form by combining data obtained from a satellite image and a DEM. We calculated channel width every ~5–7 m from a SPOT-5 satellite image (5 m resolution, *Bouillon et al.* [2006]) with the RivWidth software tool (Figure 4a) [*Pavelsky and Smith*, 2008]. We masked channels from their surroundings by exploiting the contrast between the bright bed load gravels and the flanking darker vegetation along their margins. These mapped channel widths correspond to the effective discharge that sets channel form, generates incision, and transports the largest proportion of bed load downstream in bedrock rivers [*Baker*, 1977; *Lavé and Avouac*, 2001; *Wolman and Miller*, 1960]. We measured each channel from ~1 km beyond the mountain front upstream as far as it remained visible on the satellite image (blue lines in Figure 2c).

[19] We measured channel elevation and upstream drainage area from the 90 m resolution HydroSHEDS DEM [*Lehner et al.*, 2008]. The 30 m resolution ASTER GDEM V001 and V002 [*Tachikawa et al.*, 2009] unfortunately produced major errors in the channel pathways and highly stair-stepped long profiles. We also report hillslope-scale relief from *Barnes et al.* [2011] calculated as the difference in elevation between the channel and a topographic surface interpolated between the basin boundaries and any internal high peaks. This method is a modified version of subridgeline relief introduced by *Brocklehurst and Whipple* [2002]. This hillslope relief was measured from the ASTER GDEM V001 because it has a more accurate representation of hillslope gradients than the 90 m DEM [*Barnes et al.*, 2011].

4.3. Data Integration and Calibration of Geomorphic Parameters

[20] We developed an algorithm written in the R language (version 2.15) that combines topographic information (elevation,

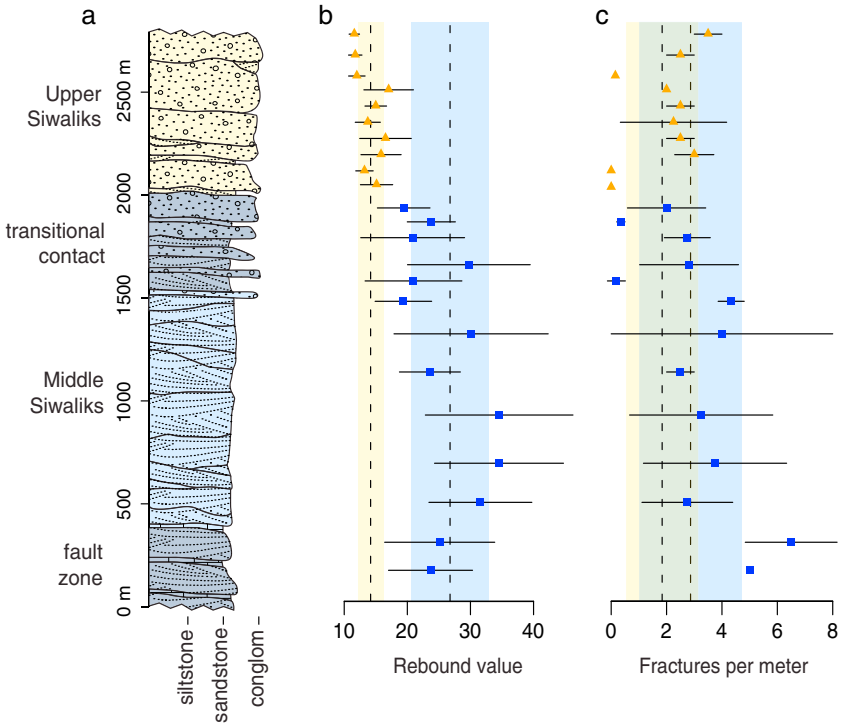

Figure 5. Siwaliks stratigraphy, intact rock strength, and fracture spacing in the Mohand range. Values are means with 1σ errors. (a) Central Mohand stratigraphic column (modified from *Kumar* [1993] and *Kumar and Nanda* [1989]). Note the transitional contact with increasing sandstone abundance down section. (b) Schmidt Hammer rebound values showing a lower mean (vertical dashed lines) intact rock strength value in the Upper Siwaliks compared to the Middle Siwaliks. This indicates the Middle Siwaliks are less erodible. (c) Fracture spacing measurements indicating no difference in mean (vertical dashed lines) spacing between the Upper and Middle Siwaliks within error. Note the increased fracturing near the mountain front associated with the HFT fault zone.

upstream drainage area, and hillslope relief) with plan view channel information (channel width, length, and sinuosity). The algorithm moves downstream and assigns data to each pixel along the image-based channel centerline from the nearest DEM pixel (Figure 4b). To reduce error, the script matches data only within the same channel and at, or downstream of, the previous DEM pixel sampled. Real channel gradients are lower than those estimated from the DEM because the 90 m resolution DEM centerline short-circuits fine-scale meanders that are visible in the higher-resolution satellite image. This method corrects for this inherent overestimation of channel slope by stretching the DEM-based elevations to the image-based channel trace.

[21] To reduce noise associated with the data integration process, we smoothed all parameters downstream using a simple moving average with a window size of 750 m (Figure B1) [after *Duvall et al.*, 2004]. Thus, we avoid interpretations at streamwise length scales <750 m. We calculated sinuosity as the ratio of channel length to straight-line distance between two endpoints spaced 1.5 km along the channel length [e.g., *Mueller*, 1968; *Stark et al.*, 2010]. We calculated channel slope at each pixel over a 12 m fixed vertical interval corresponding to the DEM accuracy [*Rabus et al.*, 2003]. In other words, we calculated slope at each pixel by comparing values located ±6 m in elevation from that pixel. We empirically determined $\theta_{ref}=0.5$ in equation (2) from the slope and drainage area data (Figure B2) and calculated normalized steepness index (k_{sn}) at every pixel downstream. Similarly, we empirically assigned $b_{ref}=0.59$ in equation (4) from the width and drainage area data (Figure B3) and calculated normalized wideness index (k_{wn}) downstream. To focus on longer length-scale patterns of channel form in plan view, we applied a second smoothing of steepness, wideness, and shear stress downstream with a 1 km simple moving average (Figure B1). Therefore, in map view, we avoid interpretations at streamwise length scales <1.75 km. Finally, when comparing geomorphic parameters between lithologies, we excluded the lithologic transition zone and took the average value of each channel for all reaches upstream of the fold axis so that averaging did not occur across lithologies and uniform rock-uplift rates could be assumed.

[22] We modeled incision potential by combining the Manning formula for a rectangular-shaped channel with the conservation of mass law to obtain the following form of the boundary shear stress equation:

$$\tau_b = \rho g \left(\frac{nQ}{W}\right)^{3/5} S^{7/10}, \tag{5}$$

where ρ is water density, g is gravity, and n is the Manning friction factor (assumed to be 0.04) [e.g., *Snyder et al.*, 2003b; *Yanites et al.*, 2010]. Because measured discharge

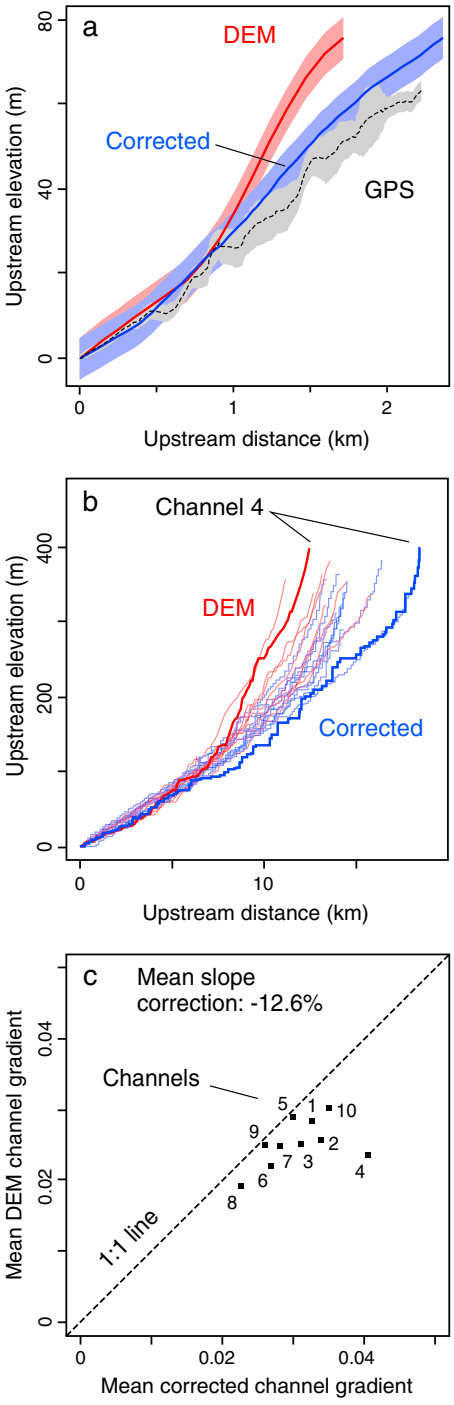

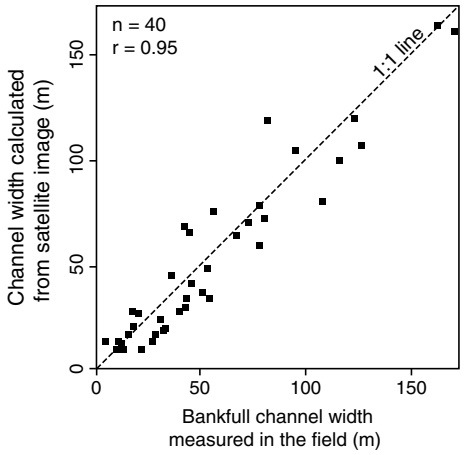

Figure 7. Comparison between image and field-based measurements of channel width. The strong correlation shows the image-based approach accurately measures true channel width in the study area.

data are unavailable for the Mohand rivers, we substituted drainage area for discharge using

$$Q = k_q A^c, \tag{6}$$

and assumed $c = 1$ and k_q is uniform on a regional scale as has been commonly demonstrated [e.g., *Hack*, 1957; *Pazzaglia et al.*, 1998] and assumed [e.g., *Duvall et al.*, 2004; *Montgomery and Gran*, 2001] for regularly shaped basins with minor orographic effects. A precipitation gradient exists within the study area [*Bookhagen and Burbank*, 2010]; however, the unavailability of discharge records necessitates the assumption of approximating c as unity although it might be lower. We eliminated the unknown coefficient k_q by normalizing each shear stress value by the maximum shear stress value calculated and creating a shear stress index, τ_{ind} that varies from 0 to 1. This index allows for comparison of relative changes in shear stress rather than absolute values.

5. Results

[23] We compare variations in lithology, channel form, and hillslope relief across the central Mohand range to factors that potentially influence channel morphology. First, we present the stratigraphy and associated erodibility of the Upper and Middle Siwaliks. Second, we validate our remote-sensing-based approach by comparing the data with field measurements. Third, we examine the spatial distribution of channel adjustment in relation to spatial variations in both lithologic changes and rock-uplift rate. Lastly, we examine correlations between several morphometrics downstream.

Figure 6. Correction and validation of DEM-based channel long profiles. (a) Example profiles estimated from the different data sets. Location is the same reach shown in Figure 4. The steeper DEM-based long profile (red) stretched to the image-based channel centerline (blue) better matches the differential GPS-based profile (black dashes) measured in the field. Swaths correspond to the vertical accuracy of the DEM and the GPS device. (b) Comparison of study area long profiles estimated from the DEM (red lines) versus those stretched to the image-based channel centerline (blue lines). Channel 4 is highlighted as the largest correction; note the stair-stepped profile showing how multiple-image-based channel centerline pixels with width values are assigned the same elevation (and drainage area) value. (c) Direct comparison of mean gradients estimated from only the DEM versus the image-corrected profiles. All corrected mean channel gradients are reduced by varying amounts depending on the channels sinuosity.

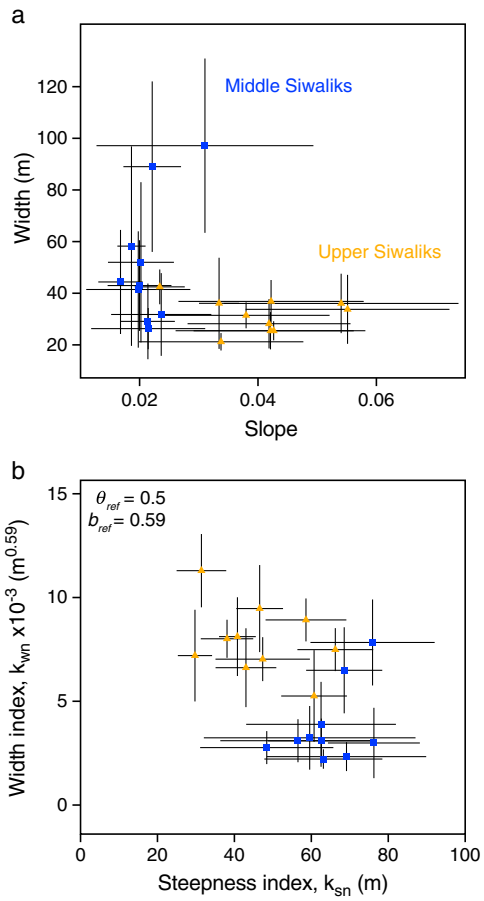

Figure 8. Comparison between channel form and rock erodibility. (a) Channel slope varies more in the Upper Siwaliks whereas width varies more in the Middle Siwaliks, partly because Middle Siwaliks channels have greater drainage areas. Values are channel means with 1σ bars, limited to the reaches above the fold axis to exclude the influence of the most major change in rock-uplift rate on channel form. See mean values in Table 1. (b) Channels have higher steepness and lower wideness in the Middle Siwaliks than in the Upper Siwaliks.

5.1. Siwalik Stratigraphy and Erodibility

[24] The Upper-to-Middle Siwaliks boundary is ~0.5 km thick, which translates to an ~1 km broad zone in map view (Figures 2 and 5). This zone contains laterally continuous meter to decameter thick conglomerate and sandstone interbeds, with the abundance of conglomerate decreasing relative to sandstone as one moves down section and downstream. Schmidt Hammer measurements show that the mean intact rock strength is 47 ± 29% greater in the Middle Siwaliks compared to the Upper Siwaliks (Figure 5). Testing by simple means confirms the same relative relationship, with mean intact rock strength of 17 ± 8 MPa for the Middle Siwaliks compared to 3 ± 3 MPa for the Upper Siwaliks. Within the transitional contact and also the upper portion of the Middle Siwaliks, intact rock strength gradually increases as the proportion of harder sandstone beds increases relative to weaker conglomerate beds. Fracture spacing is not significantly different between the two rock groups (2.9 ± 1.9 fractures/m for the Middle Siwaliks, 1.8 ± 1.3 for the Upper Siwaliks). We note an ~1 km broad HFT fault zone near the mountain front where the degree of fracturing increases. These results are consistent with previous studies that describe both formations as poorly lithified, but the Middle Siwaliks as comparatively stronger [*Kumar and Tandon*, 1985; *Kumar and Nanda*, 1989].

Table 1. Comparison of Geomorphic Parameters (Mean and 1σ) Between the Upper and Middle Siwaliks Lithologies

Geomorphic Parameter	Upper Siwaliks	Middle Siwaliks	Change
Slope	0.041 ± 0.009	0.021 ± 0.003	−49%
Width (m)	29.7 ± 6.4	51.1 ± 24.2	72%
k_{sn} (m)	46.3 ± 12.3	64.3 ± 8.6	39%
$k_{wn} \times 10^{-3}$ (m$^{0.59}$)	7.91 ± 1.74	3.80 ± 1.95	−52%
τ_{ind} excluding width	0.26 ± 0.08	0.53 ± 0.09	104%

5.2. Remote Sensing Validation

[25] Stretching the DEM-derived elevation data to the channel trace measured from the satellite image reduces channel slopes (Figure 6a). This process results in more realistic long profiles when compared to GPS measurements made in the field. The channel gradient reduction occurs in all measured channels and is proportional to the ratio between channel lengths measured from both data sources (Figure 6b). For example, highly sinuous channels that contain tight meander bends (e.g., channel 4) produce larger gradient corrections (Figures 2c and 6c). These corrections influence values of steepness index, concavity index, and shear stress and thus should be considered when using any coarse-resolution DEM to measure channels with relatively tight meander bends.

[26] Comparison of channel widths measured in the field and from the satellite image produces a strong 1:1 correlation (Figure 7). On average, there is a small bias for the remotely sensed data to underestimate true channel width by ~8% (nearly statistically significant at 95% confidence interval, p-value = 0.051). Potential sources of deviations from an exact 1:1 ratio include channel-masking errors caused by vegetation or hillsides obscuring the channel bed and registration errors between the two data sets such that differently located channel width measurements are compared. Regardless, the robust correlation (r = 0.95) between the two data sets validates our remote-sensing approach to measuring channel width continuously downstream.

5.3. Channel Form Versus Lithology

[27] Channel reaches in the weak Upper Siwaliks have a large range of mean slopes yet a small range in mean channel widths (Figure 8a and Table 1). The inverse is true for the stronger Middle Siwaliks. These results are partly a function of where each rock type is located along the channel profiles because slope and width do not necessarily vary by the same degree with increasing drainage area (e.g., Figures 1a and 1e). Thus, normalizing slope and width by drainage area, via steepness (k_{sn}) and wideness (k_{wn}) indices, produces two more comparable parameters. Channels are steeper and narrower in the Middle Siwaliks than in the Upper Siwaliks (Figure 8b and Table 1). This indicates that channels narrow and steepen in response to an increase in substrate strength, thereby focusing erosion potential to erode the stronger, uplifting rock.

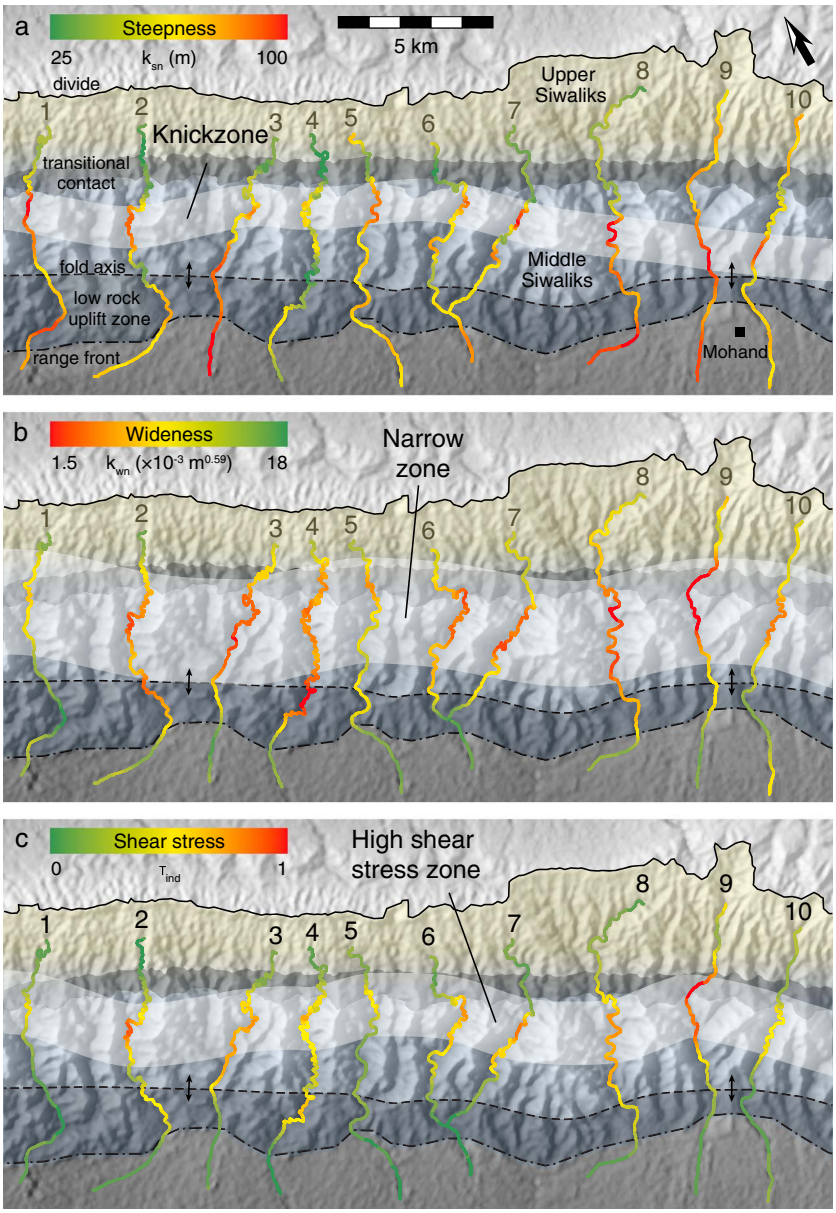

Figure 9. Plan view patterns of smoothed channel steepness, wideness, and shear stress. (a) Normalized steepness index (k_{sn}) shows an ~2 km broad knickzone oriented roughly parallel to strike within the Middle Siwaliks. (b) Normalized wideness index (k_{wn}) shows an ~4 km broad zone of narrow channels across most of the Middle Siwaliks north of the fold axis. Downstream of this zone, channels widen, often before reaching the range front. (c) Shear stress index (τ_{ind}) shows an ~3 km broad zone of high values, indicative of high relative incision potential within the Middle Siwaliks that reflects the combined effects of channel slope, width, and drainage area.

5.4. Channel Form Patterns

[28] Map-view patterns in channel steepness, wideness, and shear stress are systematic across the area. Low steepness in the Upper Siwaliks transitions to an ~2 km broad zone of high steepness (a knickzone) within the Middle Siwaliks. The position of this knickzone varies somewhat along strike (Figure 9a). All channels exhibit a narrow zone ~4 km in extent oriented along strike that begins within or near the transitional contact and ends ~1–2 km before the range front (Figure 9b). Because shear stress is a function of channel gradient, width, and upstream drainage area, its variations reflect the combined changes in steepness and wideness (Figure 9c). All channels display an ~3 km broad zone of high shear stress beginning within or near the transitional contact. Values then decrease to a minimum, often before reaching the range front.

[29] Variations in channel form downstream also exhibit systematic patterns. First, channels 1–8 reach a local steepness minimum in, or just downstream from, the transitional contact (dashed red line, Figure 10). This steepness minimum is a knickpoint location and the increase in steepness downstream is a knickzone (e.g., Figures 1c and 1d). Downstream of

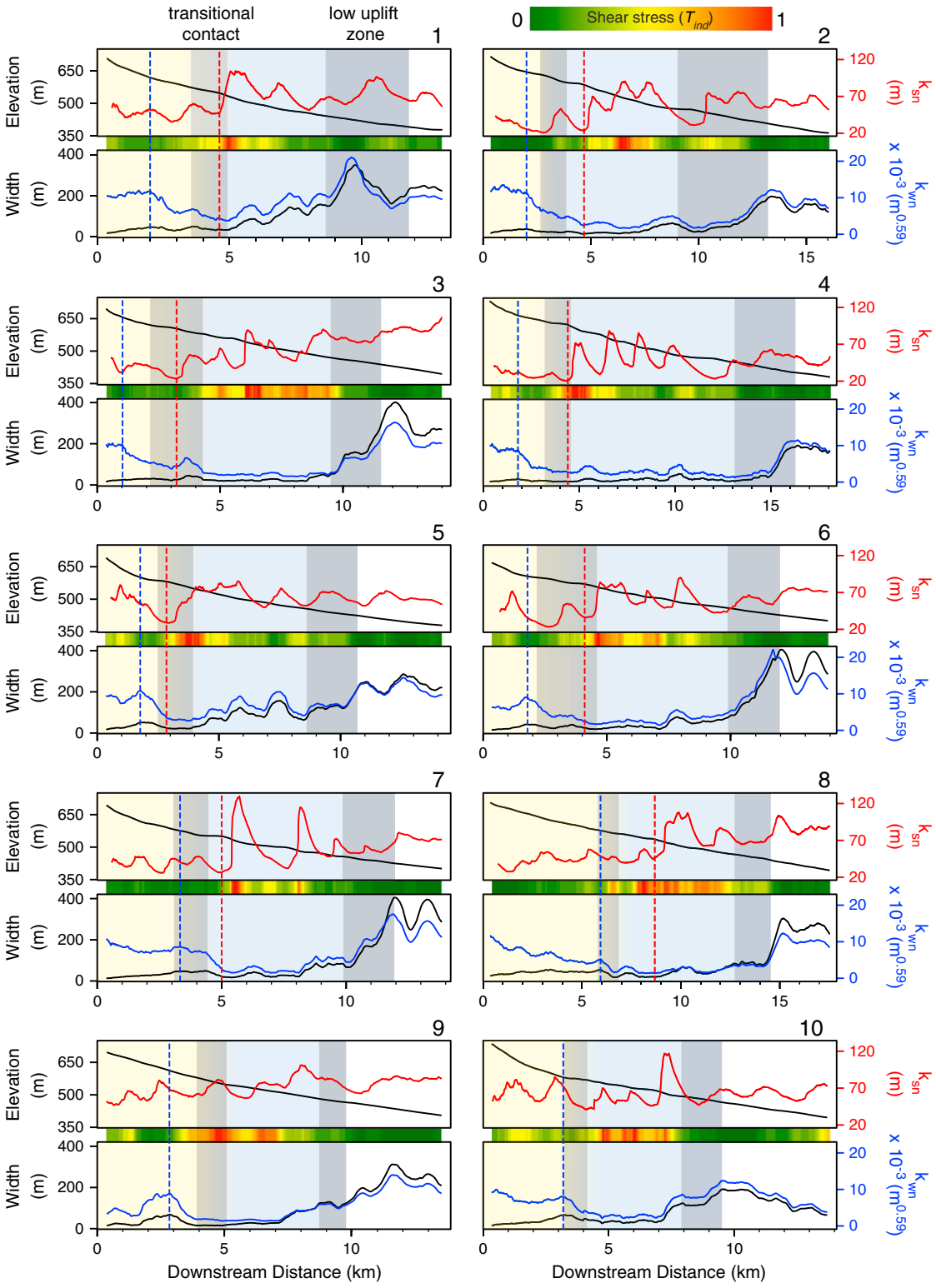

Figure 10. Downstream variations in channel form along all channels. Locations are in Figure 2c. Upstream gray bar is the Upper-to-Middle Siwaliks transitional contact and the downstream bar is the low uplift zone downstream of the fold axis within the range topography (see Figures 2b and 2c). Upper panel shows elevation profiles (black) and steepness index (k_{sn}, red); lower panel, width profiles (black) and wideness index (k_{wn}, blue). Shear stress index (τ_{ind}) is the color gradient between panels. Location of initial channel narrowing (dashed blue line) and knickpoints (dashed red line) are highlighted. All axes have the same values.

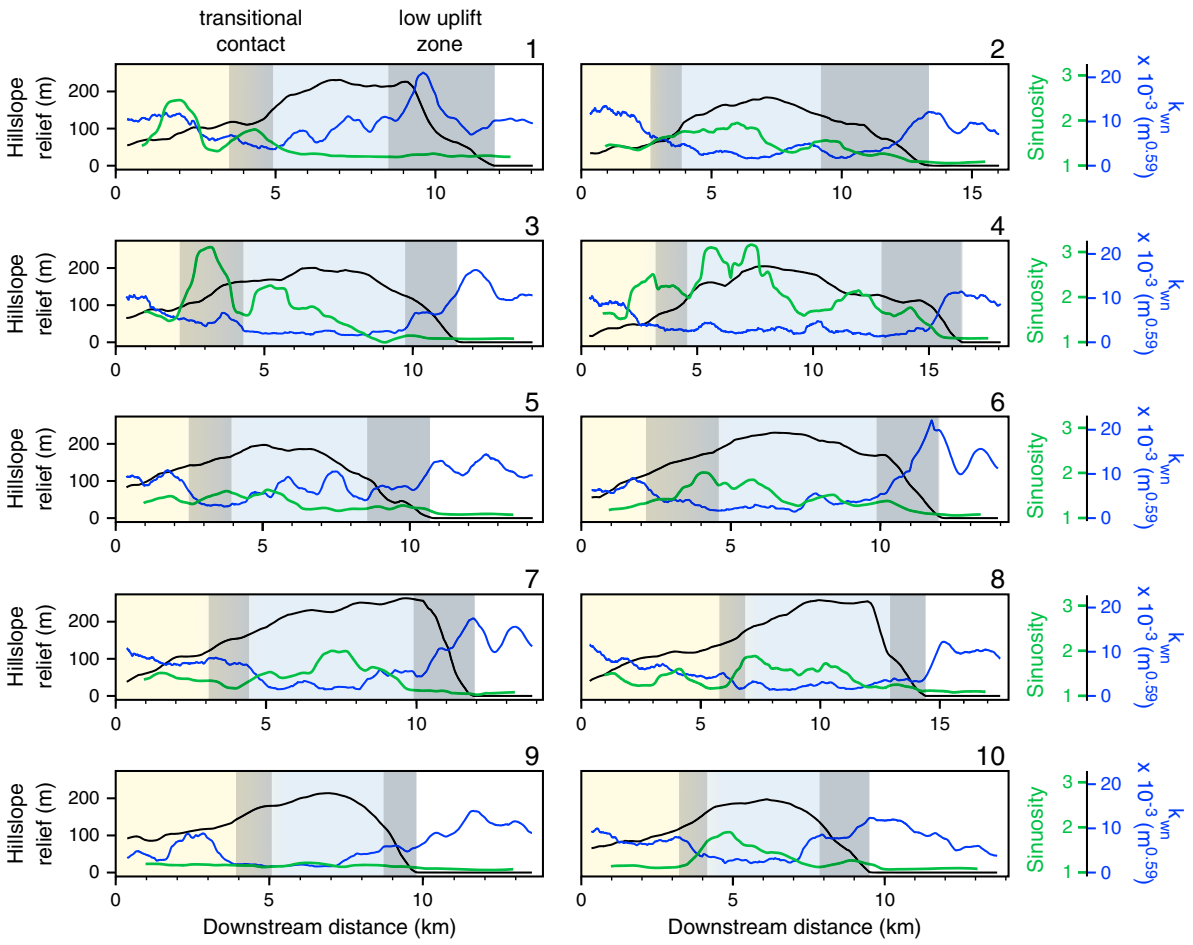

Figure 11. Downstream variations in sinuosity index (green), wideness index (k_{wn}, blue), and hillslope relief (black) along all channels. Upstream gray bar is the Upper-to-Middle Siwaliks boundary, and the downstream bar is the low uplift zone downstream of the fold axis within the range topography (see Figures 2b and 2c). Wideness inversely correlates with hillslope relief and sinuosity.

this knickzone, steepness patterns either plateau or slightly increase even beyond the range front. Second, wideness decreases downstream beginning within or just upstream from the transitional contact to near the knickpoint (dashed blue line, Figure 10). At the knickpoint, channels reach a threshold wideness minimum of $k_{wn} = \sim 5 \times 10^{-3}\ m^{0.59}$. Then, most channels (except channels 1 and 5) remain narrow until near the range front. Third, in or near the low uplift zone, channels maintain their steepness yet increase their wideness into the foreland. This width increase is the main reason for the concomitant decrease in shear stress across the low uplift zone and into the foreland. Fourth, in all channels except 1 and 9, sinuosity peaks within or just downstream from the transitional contact (Figure 11). Where sinuosity peaks, all channels except 1 and 3 are at a minimal wideness (within ~10% of the minimum).

5.5. Geomorphic Correlations

[30] Statistical comparison of spatial variations in geomorphic parameters shows that wideness is generally low where steepness, sinuosity, hillslope relief, and relative shear stress are high. Channel slope and width inversely covary

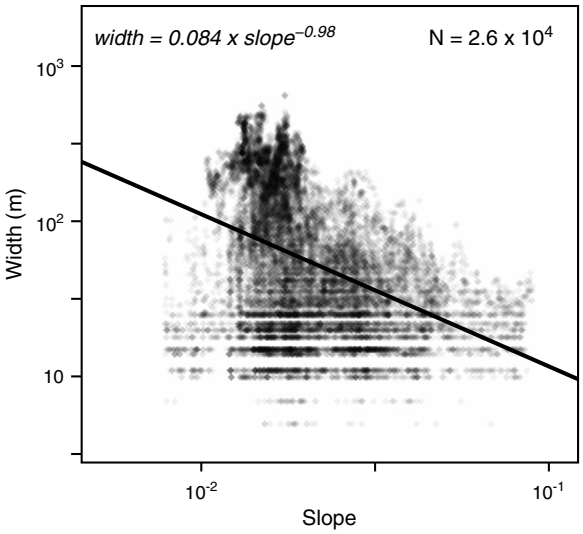

Figure 12. Channel slope versus width for all measurements. Darkness indicates higher data density. Slope-width data are highly scattered and nearly vary linearly.

Table 2. Pearson's Correlation Coefficients Between Unsmoothed Geomorphic Parameters

Channel	Slope and Width	k_{sn} and k_{wn}	k_{sn} and Sinuosity	k_{sn} and Hillslope Relief	k_{wn} and Sinuosity	k_{wn} and Hillslope Relief	Sinuosity and Hillslope Relief	τ_{ind} and Hillslope Relief	τ_{ind} and Sinuosity
1	−0.82	−0.01	−0.35	0.14	−0.07	−0.01	−0.18	0.15	0.07
2	−0.24	−0.2	−0.2	0.16	−0.52	−0.84	0.64	0.78	0.47
3	−0.40	0.45	−0.57	−0.41	−0.26	−0.91	0.28	0.83	0.02
4	−0.20	0.02	−0.1	0.36	−0.37	−0.76	0.38	0.74	0.21
5	−0.67	0.15	0.13	0.04	−0.5	−0.67	0.56	0.63	0.62
6	−0.47	0.18	−0.12	−0.08	−0.56	−0.88	0.53	0.77	0.49
7	−0.68	0.06	−0.24	0.02	−0.58	−0.84	0.41	0.57	0.34
8	−0.10	0.19	−0.2	−0.04	−0.43	−0.81	0.51	0.83	0.38
9	−0.39	0.3	−0.23	−0.17	−0.5	−0.84	0.58	0.81	0.38
10	−0.41	0.28	−0.41	−0.06	−0.63	−0.81	0.63	0.84	0.56
Mean	−0.44 ± 0.23	0.14 ± 0.17	−0.23 ± 0.18	−0.00 ± 0.20	−0.44 ± 0.16	−0.74 ± 0.25	0.43 ± 0.23	0.70 ± 0.20	0.35 ± 0.19

(Figure 12), but when they are normalized to drainage area (i.e., steepness, k_{sn} and wideness, k_{wn}), they exhibit a very low Pearson's correlation coefficient (Table 2). Slope scales as a power law function of width (higher-order polynomial fits do not significantly increase the correlation coefficient) but show a high degree of scatter. Sinuosity inversely varies with wideness while positively correlating with the relative changes in shear stress, τ_{ind}. The strongest correlation is the inverse relationship between channel wideness and hillslope relief, which holds across both Siwaliks units and the alluvial reaches beyond the mountain front (Figure 11). If our results prove to be common, this negative correlation between wideness and hillslope relief in the Mohand range hints at a potentially useful proxy for estimating channel width from DEMs.

6. Discussion

6.1. Lithologic Controls on Channel Morphology

[31] Our results show a knickpoint in most channels within or near the transitional Siwaliks boundary (Figure 10) [see also *Kirby and Whipple*, 2012]. Because we infer that rock uplift is uniform above the fault ramp, at least to a first order, these knickpoints may reflect either a transient wave of enhanced incision [e.g., *Harkins et al.*, 2007; *Whittaker et al.*, 2007], or a change in substrate erodibility [e.g., *Haviv et al.*, 2010]. It is possible that the knickpoints result from a recent increase in fault slip rate, yet the maturity of the fault system with 4–5 km of total displacement makes this scenario less likely [*Kirby and Whipple*, 2012]. Given the proximity to the change in lithology, we interpret the knickpoints to reflect the change from the weak Upper Siwaliks to the stronger Middle Siwaliks.

[32] The channels exhibit a breakdown in their slope-width ratio upstream of the knickpoints (Figure 10). We attribute this to the combined influences of a gradual downstream increase in rock strength and high sediment supply. Rivers with low sediment supply theoretically display a constant downstream relationship of $W \sim S^{-0.19}$ [*Finnegan et al.*, 2005; *Turowski et al.*, 2007]. Mohand rivers exhibit a more negative relationship of $W \sim S^{-0.98}$ (Figure 12) indicating that the sediment supply to transport capacity ratio is high [*Yanites and Tucker*, 2010]. Modeling studies predict that with high sediment supply, rivers tend to adjust their channel width more than their slope to achieve greater effective shear stress [*Finnegan et al.*, 2007; *Turowski et al.*, 2007; *Yanites and Tucker*, 2010]. Our results support this concept. As rivers traverse the Siwaliks transition zone where rock strength gradually increases, they initially maintain a balance between incision capacity and rock strength by narrowing rather than steepening their channels due to the high sediment supply. Then, as bedrock erodibility continues to decrease downstream, channel wideness reaches a minimum threshold of $\sim 5 \times 10^{-3}\ m^{0.59}$ (Figure 10), at which point we infer that further narrowing produces less efficient incision due to energy dissipation on the channel banks [*Wobus et al.*, 2006b; *Wobus et al.*, 2008; *Yanites and Tucker*, 2010]. Upon reaching a minimum width, channels instead increase their effective shear stress by steepening, resulting in the formation of a knickzone downstream (Figure 9). This pattern of narrowing upstream of steepening has already been observed where channels are adjusting to differential rock-uplift rate [*Amos and Burbank*, 2007; *Yanites et al.*, 2010], but not in response to a change in lithology.

[33] It is surprising that channel form is sensitive to changes in substrate strength given the extreme erodibility of both Siwaliks units. A physically based model proposed by Turowski et al. [2007] can solve for scaling relationships between slope and width under changing rock erodibility conditions. This model accounts for the influence of sediment cover on incision rates and assumes that rivers optimize their channel shape to minimize slope. The model predicts that weak sedimentary rocks, such as the Siwaliks, should not exert significant control on channel slope or width, a prediction not reinforced by our results. However, the prediction was made under conditions devoid of rock uplift and low sediment cover, rather than the rapid rock uplift and high sediment supply present in the Mohand. We speculate that this difference between model results and our observations implies that, all else being equal, channel geometry may be more sensitive to changes in rock erodibility with increasing rock-uplift rate and/or sediment supply.

6.2. Tectonic Controls on Channel Morphology

[34] The channels maintain their steepness yet increase their wideness values as they cross the frontal portion of the fold and transition into the foreland (Figure 10). The wideness increase may reflect the following: (1) an increase in bedrock erodibility induced by brittle deformation within the HFT fault zone [e.g., *Kumar et al.*, 2006], (2) backfilling due to increased sedimentation near the range front (i.e., alluvial sediment aggradation), and/or

(3) a decrease in rock-uplift rate. We favor the latter possibility for several reasons. First, widening begins near the Mohand fold axis, below which the HFT changes from an ~30° ramp to a flat (Figure 2b). This fault geometry corresponds to a rock-uplift rate change from ~7 to ~0 mm/yr. Second, we observed more bedrock exposures in the channel beds near the mountain front, indicating a relatively thin sediment cover, therefore reducing the likelihood of significant backfilling. Third, although rock fracturing is enhanced near the range front, thus reducing rock strength, the HFT fault zone extends only ~1 km into the range front while channel widening begins further upstream.

[35] In the Mohand, the principle geomorphic indicator of a decrease in rock-uplift rate appears to be channel width. Rivers lessen their incision capacity by changing their wideness, not necessarily their steepness (Figures 9 and 10), an observation made elsewhere in similar settings [e.g., *Lavé and Avouac*, 2001; *Montgomery and Gran*, 2001; *Yanites et al*., 2010]. The necessity to transport bed load drives rivers to maintain their long-term equilibrium long profiles across the fold axis by decreasing channel sinuosity and increasing wideness. These results imply that changes in channel width should be considered when interpreting downstream decreases in tectonic uplift from rivers with high sediment supply.

6.3. Channel Sinuosity

[36] We attribute the high channel sinuosity in the Middle Siwaliks to a combination of increased rock strength and stratigraphic interbedding under high sediment supply conditions. Channel sinuosity is a dynamic product of fluvial and hillslope processes [*Stark et al*., 2010]. Within the channel, the ratio of fluvial shear stress to channel wall strength controls the rate of lateral erosion and meander development. Outside of the channel, rock strength and climate influence hillslope stability, governing the frequency and magnitude of sediment delivery to the channel, further affecting sinuosity [*Dury*, 1954; *Stark et al*., 2010]. At the Siwaliks lithologic boundary, rivers narrow their channels to balance incision potential with the downstream increase in rock strength. A narrower river not only focuses more flow over the channel bed, it also promotes lateral erosion and channel migration by providing increased energy to wear the channel walls. Meanders form when the lateral migration rate of a channel's inner bank matches that of the outer bank [*Finnegan and Dietrich*, 2011]. As is the case in Mohand, this process occurs by sedimentary aggradation on the inner bank and/or by the river slipping off the inner bank as the channel bed and outer bank are incised. Channels widen at the fold axis, presumably in response to the decrease in rock-uplift rate that reduces both vertical and lateral incision. This widening in turn reduces channel lateral migration, resulting in the observed reduction in sinuosity.

[37] The observed sinuosity patterns may also result from the Mohand stratigraphy. Field observations show that rivers flowing against dip tend to exhibit higher sinuosity than those flowing downdip [*Harden*, 1990]. This is because weaker interbeds promote lateral erosion, causing channels to preferentially align parallel to strike, whereas stronger beds tend to resist lateral erosion, directing the channel across strike. While all studied rivers in the Mohand flow across dip, reaches in the upper Middle Siwaliks traverse through sandstone and conglomerate interbeds with highly variable strength (Figure 5). The spatial coincidence between meter to decameter thick interbeds and increased meander development in the Mohand implies the former may cause the latter. We suggest that small-scale stratigraphic variations in rock strength within a single geologic unit may affect observable changes in bedrock channel form.

6.4. Possible Role of Variable Rock Uplift

[38] We have assumed that rock-uplift rate is uniform across the study area save for the transition from the HFT ramp to flat near the mountain front. The best estimate for more detailed changes in relative rock-uplift rate is from a balanced cross section that implies three small kinks in the fault ramp translating into several different uplift zones (Figure 2b) [*Barnes et al*., 2011; *Mishra and Mukhopadhyay*, 2002]. Unfortunately, the locations of these kinks are approximate [*Mishra and Mukhopadhyay*, 2002]. Regardless, from the drainage divide to the ramp flat, rock-uplift rates range from ~6.9 to ~8.2 mm/yr, translating into an average increase of ~16% downstream. It is possible the rivers may be adjusting their width as they flow into the Middle Siwaliks in response to this subtle increase in relative rock uplift, rather than entirely due to the increase in rock strength. Similarly, patterns of relief, sinuosity, and slope may all be responding, at least in part, to these variations. While recognizing this possibility, we favor lithology as the principle control of channel form change here because of the strong spatial coincidence between the Upper to Middle Siwaliks transition with major morphometric changes.

7. Conclusions

[39] Bedrock river form reflects changes in rock strength and rock-uplift rate across the Mohand range at the Himalayan front when both channel widths and slopes are explicitly considered. Here where channels are in near-equilibrium conditions and sediment supply is high, we make the following conclusions: (1) rivers respond to downstream variations in rock strength and rock-uplift rate by adjusting their channel widths upstream of, and to a greater degree than, the adjustments of their slopes; (2) channel geometry may be more sensitive to changes in rock strength with increasing rock-uplift rate; (3) increased rock strength enhances river meander formation by narrowing channels, thereby increasing lateral erosion; and (4) rivers flowing across alternating strong and weak stratigraphic interbeds exhibit increased sinuosity, suggesting that variability in bedrock strength via sedimentary interbedding can influence river slope, steepness, concavity, and shear stress. We also find that channel slope is overestimated where meanders are finer scale than DEM resolution. Finally, this study highlights the importance of rock strength, sediment supply, and stratigraphic variations in influencing channel form and hence advocates for including channel width measurements when trying to extract tectonic signals from bedrock rivers.

Appendix A: Wideness Index Derivation

[40] The wideness index can be used as an empirical measure of deviation from an equilibrium width-area scaling, but it can also be related to incision potential. Derivation of

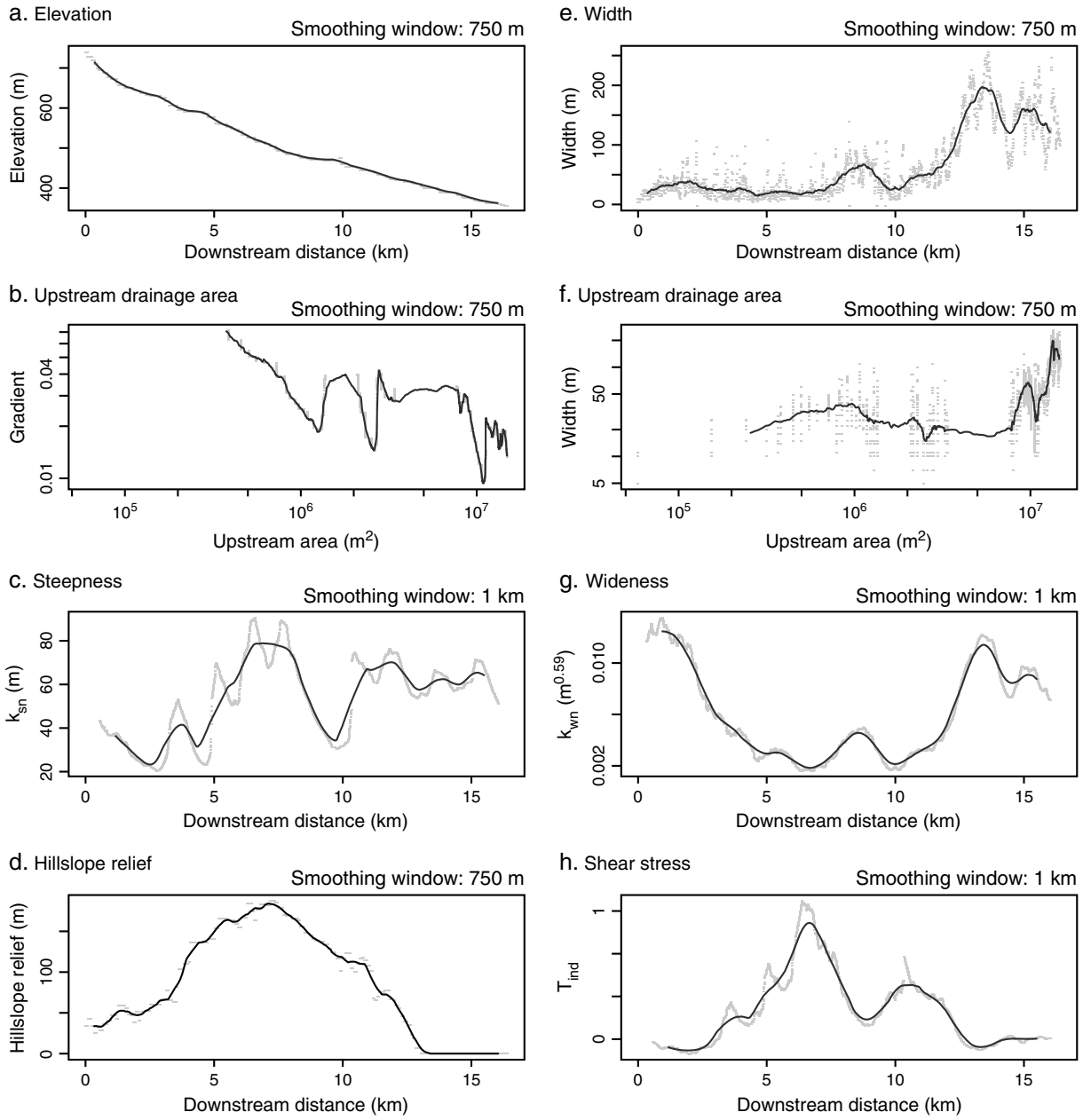

Figure B1. Example channel (2 in Figure 2c) showing raw (gray) and smoothed (black) data. (a) Elevation, (b, f) upstream drainage area, (d) hillslope relief, and (e) width were smoothed with a 750 m simple moving average (Figures 10 and 11) [after *Duvall et al*., 2004]. (c) Steepness (k_{sn}), (h) wideness (k_{wn}), and shear stress (τ_{ind}) indices with a 1 km simple moving average, a necessary window length for displaying large-scale trends in plan view (Figure 9).

the wideness index closely follows that of the steepness index [see *Duvall et al*., 2004, appendix; *Whipple and Tucker*, 1999]. However, rather than assuming channel width scales with drainage area, we rely on the fact that channel slope exhibits an equilibrium scaling with drainage area as described in equation (1). The wideness index is derived from the stream-power family of models that equate bedrock incision rate (E) to a power function of boundary shear stress (τ_b) that must exceed a threshold of critical shear stress (τ_c):

$$E = k_e f(q_s)[\tau_b - \tau_c]^{a_e}, \tag{A1}$$

where k_e depends on rock erodibility, $f(q_s)$ describes the dual role entrained sediment plays as both tools and cover for incision, and a_e depends on the erosion mechanics [*Howard and Kerby*, 1983; *Whipple et al*., 2000]. This is true assuming that the influence of critical shear stress (τ_c) is negligible because (a) the effective discharge that shapes bedrock channels typically far exceeds this value in the Siwalik Hills [*Kirby and Whipple*, 2012] and (b) sediment flux scales with shear stress [*Bagnold*, 1980].

[41] Incision rate is reduced to terms of boundary shear stress, which under steady-uniform flow can be approximated in terms of channel discharge, width, and slope:

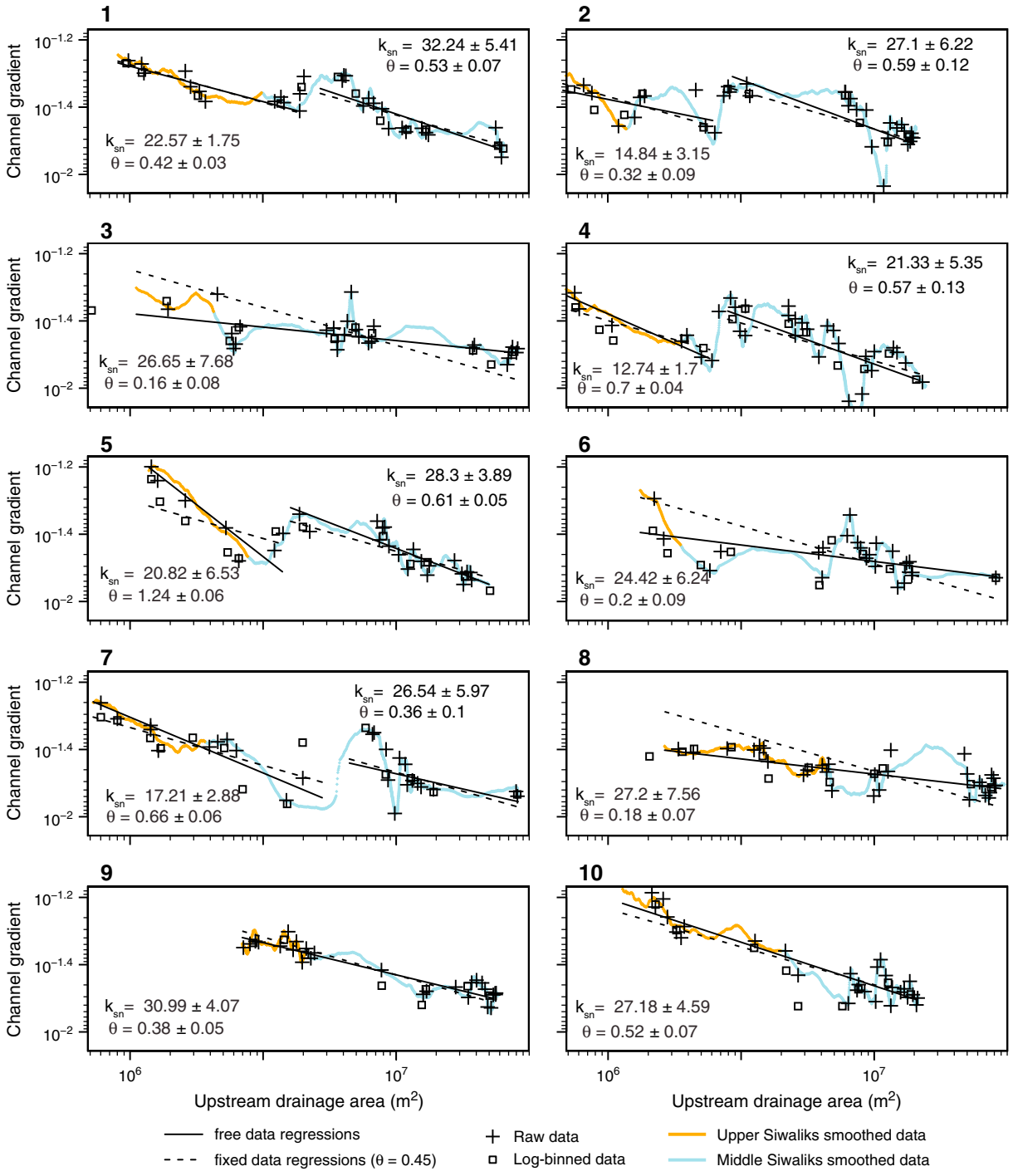

Figure B2. Channel slope versus drainage area for all 10 channels. Lines are regression limits applied to the equilibrium reaches. Normalized steepness index values are calculated with a 0.45 reference concavity. Average concavity indices: Upper Siwaliks = 0.48, Middle Siwaliks = 0.41, and all equilibrium channel reaches = 0.5.

$$\tau_b = k_t Q^{\alpha} W^{-\alpha} S^{\beta}, \tag{A2}$$

where k_t, α, and β are constants that depend on flow resistance dynamics [e.g., *Yanites et al.*, 2010]. Combining equations (1), (6), (A1), and (A2) yields

$$E = K' A^{m'} W^{-n'}, \tag{A3a}$$

where

$$K' = k_e f(q_s) \left(k_t k_q^{\alpha} k_s^{\beta} \right)^{a_e}, \tag{A3b}$$

$$m' = a_e (c\alpha - \theta\beta), \tag{A3c}$$

$$n' = \alpha a_e. \tag{A3d}$$

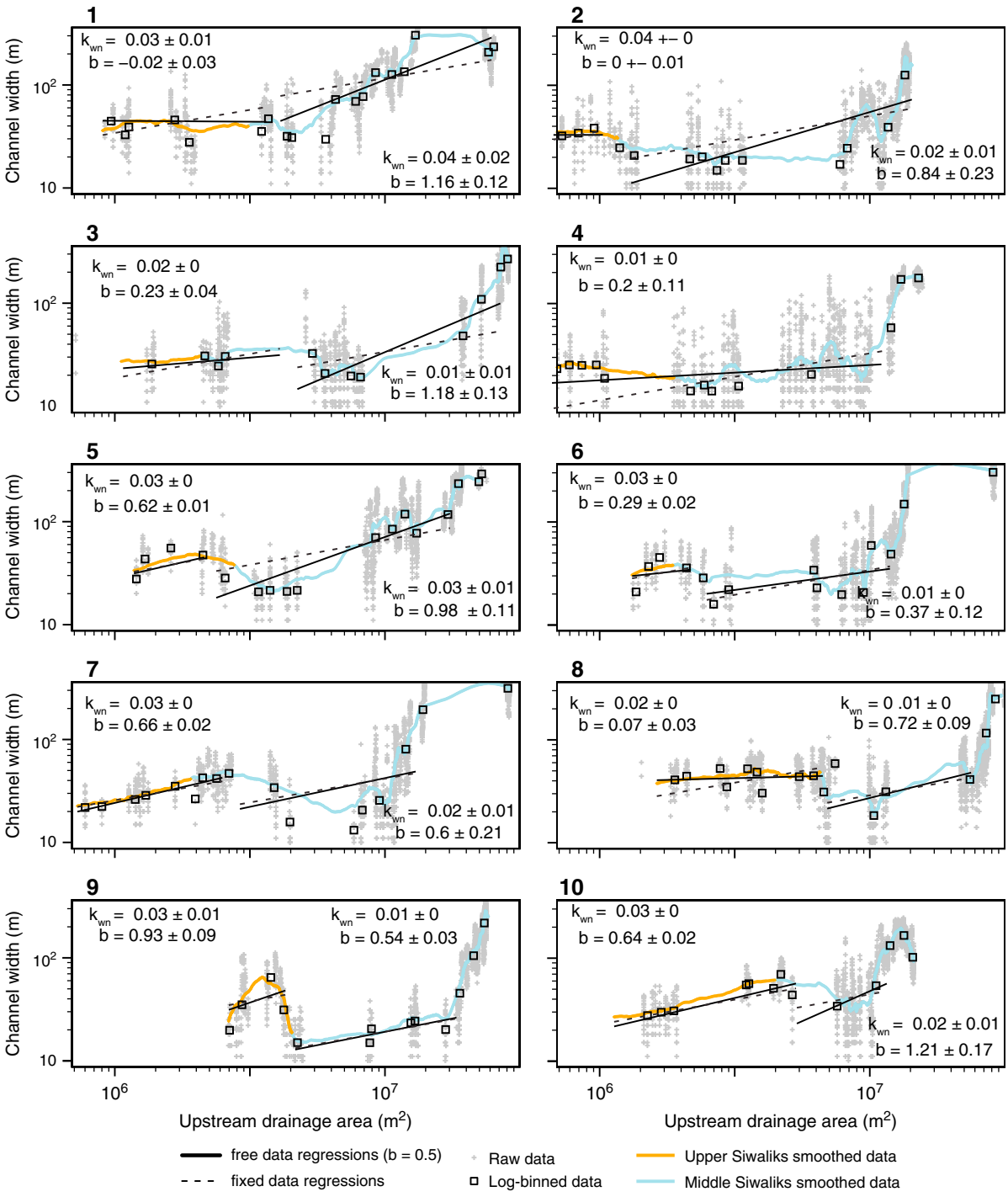

Figure B3. Channel width versus drainage area for all channels. Most channels narrow downstream beyond the transitional contact then widen before the range front. Lines show regression limits applied to equilibrium reaches. Normalized wideness index values are calculated using a 0.5 reference width exponent. Mean width exponents: Upper Siwaliks = 0.36, Middle Siwaliks = 0.72, and all equilibrium channel reaches = 0.59.

[42] Equation (A3a) resembles the form of the generalized total stream-power model [*Howard and Kerby*, 1983] except in terms of channel width rather than slope.

[43] If steady state equilibrium conditions exist such that long term rock-uplift rate (U) and bedrock incision rate are balanced and the channel bed elevation does not vary with time ($\frac{dz}{dt} = 0$), then

$$U = E = K' A^{m'} W_e^{-n'}, \tag{A4}$$

which can be rearranged to solve for equilibrium channel width:

$$W_e = (U/K')^{-1/n'} A^{m'/n'}. \quad \text{(A5)}$$

[44] This takes the form similar to the width-area formula of equation (3):

$$W = k_w A^b, \quad \text{(A6a)}$$

where k_w is the wideness index and b is the width exponent with the implied relations

$$k_w = (U/K')^{-1/n'} \quad \text{(A6b)}$$

and

$$b = m'/n'. \quad \text{(A6c)}$$

[45] The width exponent can be empirically determined by plotting channel width and drainage area in log-log space and taking linear regressions of channel reaches that exhibit a steady power law widening (Appendix B).

Appendix B: Data Smoothing and Empirical Determination of Exponents

[46] DEM pixels were sampled unevenly in the data integration process resulting in a stair-stepped pattern on the elevation profiles in the image-corrected data set because the data sources were at different resolutions (Figure 6b). This stair-step effect, combined with occasional misalignment of tributary junctions between the DEM and image, requires some smoothing of the morphometric variables to reduce noise. We initially smoothed channel elevation, width, upstream drainage area, and hillslope relief data using a downstream simple moving average with a window size of 750 m (Figures B1a, B1b, and B1d–B1f) [after *Duvall et al.*, 2004]. We then determined the reference concavity index and width exponent by taking the average slope of linear regressions fit to all equilibrium channel reaches (Figures B2 and B3) and calculated steepness and wideness indices at every pixel using $\theta_{ref} = 0.5$ and $b_{ref} = 0.59$. Figure 9 shows smoothed normalized steepness, wideness, and shear stress indices using a simple moving average with a window size of 1 km downstream distance, a length necessary to focus on only the large-scale variations in channel shape (Figures B1c, B1g, and B1h).

[47] **Acknowledgments.** We thank Vikrant Jain, Vimal Singh, Aravind Nair, Rakesh Malhotra, and K.K. Sharma for help with the fieldwork and logistics. Jonathan Lees provided analytical advice and Rajiv Sinha provided the Spot 5 image. Financial support was provided by NSF EAR 0814723 to J. Barnes and by the UNC Geological Sciences Martin Fund and a GSA Graduate Research Grant to G. Allen. We also thank Brian Yanites, two anonymous reviewers, and associate editor Simon Brocklehurst for their helpful comments on this paper.

References

Amos, C. B., and D. W. Burbank (2007), Channel width response to differential uplift, *J. Geophys. Res.*, *112*, F02010, doi:10.1029/2006JF000672.

Anderson, R. S. (1994), Evolution of the Santa Cruz Mountains, California, through tectonic growth and geomorphic decay, *J. Geophys. Res.*, *99*(B10), 20,161–20,179, doi:10.1029/94JB00713.

Bagnold, R. A. (1980), An Empirical Correlation of Bedload Transport Rates in Flumes and Natural Rivers, *Proc. R. Soc. Lond. Ser. A, Math*, *372*(1751), 453–473, doi:10.1098/rspa.1980.0122.

Baker, V. R. (1977), Stream-channel response to floods, with examples from central Texas, *Geol. Soc. Am. Bull.*, *88*(8), 1057–1071, doi:10.1130/0016-7606(1977)88<1057:srtfwe>2.0.co;2.

Barnes, J. B., A. L. Densmore, M. Mukul, R. Sinha, V. Jain, and S. K. Tandon (2011), Interplay between faulting and base level in the development of Himalayan frontal fold topography, *J. Geophys. Res.*, *116*, F03012, doi:10.1029/2010JF001841.

Bilham, R., K. Larson, and J. Freymueller (1997), GPS measurements of present-day convergence across the Nepal Himalaya, *Nature*, *386*(6620), 61–64, doi:10.1038/386061a0.

Bookhagen, B., and D. W. Burbank (2006), Topography, relief, and TRMM-derived rainfall variations along the Himalaya, *Geophys. Res. Lett.*, *33*, L08405, doi:10.1029/2006GL026037.

Bookhagen, B., and D. W. Burbank (2010), Toward a complete Himalayan hydrological budget: Spatiotemporal distribution of snowmelt and rainfall and their impact on river discharge, *J. Geophys. Res.*, *115*, F03019, doi:10.1029/2009JF001426.

Bouillon, A., M. Bernard, P. Gigord, A. Orsoni, V. Rudowski, and A. Baudoin (2006), SPOT 5 HRS geometric performances: Using block adjustment as a key issue to improve quality of DEM generation, *ISPRS J. Photogram. Rem. Sens.*, *60*(3), 134–146, doi:10.1016/j.isprsjprs.2006.03.002.

Brocklehurst, S. H., and K. X. Whipple (2002), Glacial erosion and relief production in the Eastern Sierra Nevada, California, *Geomorphology*, *42*(1–2), 1–24, doi:10.1016/s0169-555x(01)00069-1.

Burbank, D. W., J. Leland, E. Fielding, R. S. Anderson, N. Brozovic, M. R. Reid, and C. Duncan (1996), Bedrock incision, rock uplift and threshold hillslopes in the northwestern Himalayas, *Nature*, *379*(6565), 505–510, doi:10.1038/379505a0.

Cargill, J. S., and A. Shakoor (1990), Evaluation of empirical methods for measuring the uniaxial compressive strength of rock, *Int. J.Rock Mech. Min Sci. & Geomech. Abstr.*, *27*(6), 495–503, doi:10.1016/0148-9062(90)91001-n.

Clarke, B. A., and D. W. Burbank (2011), Quantifying bedrock-fracture patterns within the shallow subsurface: Implications for rock mass strength, bedrock landslides, and erodibility, *J. Geophys. Res.*, *116*, F04009, doi:10.1029/2011JF001987.

Cyr, A. J., D. E. Granger, V. Olivetti, and P. Molin (2010), Quantifying rock uplift rates using channel steepness and cosmogenic nuclide–determined erosion rates: Examples from northern and southern Italy, *Lithosphere*, *2*(3), 188–198, doi:10.1130/l96.1.

Dühnforth, M., R. S. Anderson, D. Ward, and G. M. Stock (2010), Bedrock fracture control of glacial erosion processes and rates, *Geology*, *38*(5), 423–426, doi:10.1130/g30576.1.

Dury, G. H. (1954), Contribution to a general theory of meandering valleys, *Am. J. Sci.*, *252*(4), 193–224, doi:10.2475/ajs.252.4.193.

Duvall, A., E. Kirby, and D. Burbank (2004), Tectonic and lithologic controls on bedrock channel profiles and processes in coastal California, *J. Geophys. Res.*, *109*, F03002, doi:10.1029/2003JF000086.

England, P., and P. Molnar (1997), Active Deformation of Asia: From Kinematics to Dynamics, *Science*, *278*(5338), 647–650, doi:10.1126/science.278.5338.647.

Finnegan, N. J., and W. E. Dietrich (2011), Episodic bedrock strath terrace formation due to meander migration and cutoff, *Geology*, *39*(2), 143–146, doi:10.1130/g31716.1.

Finnegan, N. J., G. Roe, D. R. Montgomery, and B. Hallet (2005), Controls on the channel width of rivers: Implications for modeling fluvial incision of bedrock, *Geology*, *33*(3), 229–232, doi:10.1130/g21171.1.

Finnegan, N. J., L. S. Sklar, and T. K. Fuller (2007), Interplay of sediment supply, river incision, and channel morphology revealed by the transient evolution of an experimental bedrock channel, *J. Geophys. Res.*, *112*, F03S11, doi:10.1029/2006JF000569.

Flint, J. J. (1974), Stream gradient as a function of order, magnitude, and discharge, *Water Resour. Res.*, *10*(5), 969–973, doi:10.1029/WR010i005p00969.

Gallen, S. F., K. W. Wegmann, and D. R. Bohnenstieh (2013), Miocene rejuvenation of topographic relief in the southern Appalachians, *GSA Today*, *23*(2), 4–10, doi:10.1130/GSATG163A.1.

Gilbert, G. K. (1877), Report on the Geology of the Henry Mountains, Dept. of the Interior, US Geographical and Geological Survey of the Rocky Mountain Region, Washington, D.C.

Gillespie, P. A., C. B. Howard, J. J. Walsh, and J. Watterson (1993), Measurement and characterisation of spatial distributions of fractures, *Tectonophysics*, *226*(1–4), 113–141, doi:10.1016/0040-1951(93)90114-Y.

Goode, J. R., and E. Wohl (2010), Substrate controls on the longitudinal profile of bedrock channels: Implications for reach-scale roughness, *J. Geophys. Res.*, *115*, F03018, doi:10.1029/2008JF001188.

Goudie, A. S. (2006), The Schmidt Hammer in geomorphological research, *Prog. Phys. Geog.*, *30*(6), 703–718, doi:10.1177/0309133306071954.

Gupta, S., and M. A. Ellis (2004), Does the topography of actively growing folds mimic fold structure? the case of the Mohand anticline, frontal Himalaya, *Geophys. Res. Abstr.*, 606,593.

Hack, J. T. (1957), Studies of longitudinal stream profiles in Virginia and Maryland, *US Geol. Surv. Prof. Pap.*, pp. 45–97.

Hack, R., and M. Huisman (2002), Estimating the intact rock strength of a rock mass by simple means, in *9th Congr.of the Int. Ass. Engin. Geol. Env*, edited by J. L. van Rooy and C. A. Jermy, Engineering Geology for Developing Countries, Durban, South Africa.

Hancock, G. S., E. E. Small, and C. Wobus (2011), Modeling the effects of weathering on bedrock-floored channel geometry, *J. Geophys. Res.*, *116*, F03018, doi:10.1029/2010JF001908.

Harbor, D. J. (1998), Dynamic Equilibrium between an Active Uplift and the Sevier River, Utah, *J. Geol.*, *106*(2), 181–194, doi:10.1086/516015.

Harden, D. R. (1990), Controlling factors in the distribution and development of incised meanders in the central Colorado Plateau, *Geol. Soc. Am. Bull.*, *102*(2), 233–242, doi:10.1130/0016-7606(1990)102<0233:CFITDA>2.3.CO;2.

Harkins, N., E. Kirby, A. Heimsath, R. Robinson, and U. Reiser (2007), Transient fluvial incision in the headwaters of the Yellow River, northeastern Tibet, China, *J. Geophys. Res.*, *112*, F03S04, doi:10.1029/2006JF000570.

Haviv, I., Y. Enzel, K. X. Whipple, E. Zilberman, A. Matmon, J. Stone, and K. L. Fifield (2010), Evolution of vertical knickpoints (waterfalls) with resistant caprock: Insights from numerical modeling, *J. Geophys. Res.*, *115*, F03028, doi:10.1029/2008JF001187.

Howard, A. D. (1994), A detachment-limited model of drainage basin evolution, *Water Resour. Res.*, *30*(7), 2261–2285, doi:10.1029/94WR00757.

Howard, A. D., and G. Kerby (1983), Channel changes in badlands, *Geol. Soc. Am. Bull.*, *94*(6), 739–752, doi:10.1130/0016-7606(1983)94<739:CCIB>2.0.CO;2.

Howard, A. D., W. E. Dietrich, and M. A. Seidl (1994), Modeling fluvial erosion on regional to continental scales, *J. Geophys. Res.*, *99*(B7), 13,971–13,986, doi:10.1029/94JB00744.

Kirby, E., and K. Whipple (2001), Quantifying differential rock-uplift rates via stream profile analysis, *Geology*, *29*(5), 415–418, doi:10.1130/0091-7613(2001)029<0415:qdrurv>2.0.co;2.

Kirby, E., and K. X. Whipple (2012), Expression of active tectonics in erosional landscapes, *J. Struct. Geol.*, doi:10.1016/j.jsg.2012.07.009.

Kumar, R. (1993), Coalescence megafan: multistorey sandstone complex of the late-orogenic (Mio-Pliocene) sub-Himalayan belt, Dehra Dun, India, *Sed. Geol.*, *85*(1–4), 327–337, doi:10.1016/0037-0738(93)90091-i.

Kumar, R., and S. K. Ghosh (1991), Sedimentological Studies of the Upper Siwalik Boulder Conglomerate Formation, Mohand Area, District Saharampur, U.P, *J. Himal. Geol.*, *2*(2), 159–167.

Kumar, R., and A. C. Nanda (1989), Sedimentology of the Middle Siwalik Subgroup of Mohand area, Dehra Dun Valley, India, *J. Geol. Soc. India*, *34*(6), 597–616.

Kumar, R., and S. K. Tandon (1985), Sedimentology of Plio-Pleistocene late orogenic deposits associated with intraplate subduction—the Upper Siwalik Subgroup of a part of Panjab Sub-Himalaya, India, *Sed. Geol.*, *42*(1–2), 105–158, doi:10.1016/0037-0738(85)90076-4.

Kumar, S., S. G. Wesnousky, T. K. Rockwell, D. Ragona, V. C. Thakur, and G. G. Seitz (2001), Earthquake Recurrence and Rupture Dynamics of Himalayan Frontal Thrust, India, *Science*, *294*(5550), 2328–2331, doi:10.1126/science.1066195.

Kumar, S., S. G. Wesnousky, T. K. Rockwell, R. W. Briggs, V. C. Thakur, and R. Jayangondaperumal (2006), Paleoseismic evidence of great surface rupture earthquakes along the Indian Himalaya, *J. Geophys. Res.*, *111*, doi:10.1029/2004JB003309.

Lavé, J., and J. P. Avouac (2000), Active folding of fluvial terraces across the Siwaliks Hills, Himalayas of central Nepal, *J. Geophys. Res.*, *105*(B3), 5735–5770, doi:10.1029/1999JB900292.

Lavé, J., and J. P. Avouac (2001), Fluvial incision and tectonic uplift across the Himalayas of central Nepal, *J. Geophys. Res.*, *106*(B11), 26,561–26,591, doi:10.1029/2001JB000359.

Lehner, B., K. Verdin, and A. Jarvis (2008), New Global Hydrography Derived From Spaceborne Elevation Data, *Eos. Trans. AGU*, *89*(10), doi:10.1029/2008EO100001.

Leopold, L. B., and T. Maddock, Jr. (1953), The hydraulic geometry of stream channels and some physiographic implications, *US Geol. Surv. Prof. Pap. 252*, 6 pp.

Malik, J. N., and T. Nakata (2003), Active faults and related Late Quaternary deformation along the Northwestern Himalayan Frontal Zone, India, *Annal. Geophys.*, *46*(5), 917–936, doi: 2122/996.

Mishra, P., and D. K. Mukhopadhyay (2002), Balanced structural models of Mohand and Santaurgarh ramp anticlines, Himalayan foreland fold-thrust belt, Dehra Dun re-entrant, Uttaranchal, *J. Geol. Soc. India*, *60*(6), 649–661.

Mohindra, R., B. Parkash, and J. Prasad (1992), Historical geomorphology and pedology of the Gandak Megafan, Middle Gangetic Plains, India, *Earth Surf. Processes Landforms*, *17*(7), 643–662, doi:10.1002/esp.3290170702.

Molnar, P., and P. England (1990), Late Cenozoic uplift of mountain ranges and global climate change: chicken or egg?, *Nature*, *346*(6279), 29–34, doi:10.1038/346029a0.

Montgomery, D. R., and M. T. Brandon (2002), Topographic controls on erosion rates in tectonically active mountain ranges, *Earth Planet. Sci. Lett.*, *201*(3–4), 481–489, doi:10.1016/s0012-821x(02)00725-2.

Montgomery, D. R., and K. B. Gran (2001), Downstream variations in the width of bedrock channels, *Water Resour. Res.*, *37*(6), 1841–1846, doi:10.1029/2000WR900393.

Montgomery, D. R., T. B. Abbe, J. M. Buffington, N. P. Peterson, K. M. Schmidt, and J. D. Stock (1996), Distribution of bedrock and alluvial channels in forested mountain drainage basins, *Nature*, *381*(6583), 587–589, doi:10.1038/381587a0.

Mueller, J. E. (1968), An Introduction to the Hydraulic and Topographic Sinuosity Indexes, *Annal. Ass. Am. Geog.*, *58*(2), 371–385, doi:10.1111/j.1467-8306.1968.tb00650.x.

Nakata, T. (1989), Active faults of the Himalaya of India and Nepal, in *Tectonics of the Western Himalayas*, edited by L. L. Malinconico and R. J. Lillie, *Spec. Pap. Geol. Soc. Am.*, *232*, 243–264.

Ouimet, W. B., K. X. Whipple, and D. E. Granger (2009), Beyond threshold hillslopes: Channel adjustment to base-level fall in tectonically active mountain ranges, *Geology*, *37*(7), 579–582, doi:10.1130/g30013a.1.

Pavelsky, T. M., and L. C. Smith (2008), RivWidth: A Software Tool for the Calculation of River Widths From Remotely Sensed Imagery, *Geosci. Remote Sens. Lett., IEEE*, *5*(1), 70–73, doi:10.1109/lgrs.2007.908305.

Pazzaglia, F. J., T. W. Gardner, and D. J. Merritts (1998), Bedrock fluvial incision and longitudinal profile development over geologic time scales determined by fluvial terraces, in *Rivers Over Rock: Fluvial Processes in Bedrock Channels*, edited by K. J. Tinkler, and E. E. Wohl, pp. 207–235, AGU, Washington, DC.

Powers, P. M., R. J. Lillie, and R. S. Yeats (1998), Structure and shortening of the Kangra and Dehra Dun reentrants, Sub-Himalaya, India, *Geol. Soc. Am. Bull.*, *110*(8), 1010–1027, doi:10.1130/0016-7606(1998)110<1010:sasotk>2.3.co;2.

Rabus, B., M. Eineder, A. Roth, and R. Bamler (2003), The shuttle radar topography mission--a new class of digital elevation models acquired by spaceborne radar, *ISPRS J. Photogramm.*, *57*(4), 241–262, doi:10.1016/S0924-2716(02)00124-7.

Raiverman, V., A. Mukerjea, M. K. Saproo, S. V. Kunte, and J. Ram (1990), Geological map of Himalayan foothills between Yamuna and Sarda rivers, Keshava Deva Malaviya Institute of Petrolium Exploration, Oil and Natural Gas Corporation, Dehra Dun, India.

Rao, Y. S. N., A. A. Rahman, and D. P. Rao (1975), On the structure of the Siwalik Range between the rivers Yamuna and Ganga, *Himalayan Geology*, *4*, 137–150.

Safran, E. B., P. R. Bierman, R. Aalto, T. Dunne, K. X. Whipple, and M. W. Caffee (2005), Erosion rates driven by channel network incision in the Bolivian Andes, *Earth Surf. Proc. Land. 30*, 1007–1024, doi:10.1002/esp.1259.

Sangode, S. J., and R. Kumar (2003), Magnetostratigraphic correlation of the Late Cenozoic fluvial sequences from NW Himalaya, India, *Curr. Sci. India*, *84*(8), 1014–1024.

Selby, M. J. (1993), *Hillslope Materials and Processes*, Oxford University Press, Oxford, UK, 2nd ed.

Sklar, L., and W. E. Dietrich (1998), River longitudinal profiles and bedrock incision models: Stream power and the influence of sediment supply, in *Rivers Over Rock: Fluvial Processes in Bedrock Channels*, Geophys. Monogr. Ser., vol. 107, edited by K. J. Tinkler and E. E. Wohl, pp. 237–260, AGU, Washington, D. C.

Sklar, L. S., and W. E. Dietrich (2001), Sediment and rock strength controls on river incision into bedrock, *Geology*, *29*(12), 1087–1090.

Sklar, L. S., and W. E. Dietrich (2004), A mechanistic model for river incision into bedrock by saltating bed load, *Water Resour. Res.*, *40*, W06301, doi:10.1029/2003WR002496.

Snyder, N. P., K. X. Whipple, G. E. Tucker, and D. J. Merritts (2003a), Channel response to tectonic forcing: field analysis of stream morphology and hydrology in the Mendocino triple junction region, northern California, *Geomorphology*, *53*(1–2), 97–127, doi:10.1016/s0169-555x(02)00349-5.

Snyder, N. P., K. X. Whipple, G. E. Tucker, and D. J. Merritts (2003b), Importance of a stochastic distribution of floods and erosion thresholds in the bedrock river incision problem, *J. Geophys. Res.*, *108*(B2), 2117, doi:10.1029/2001JB001655.

Stark, C. P. (2006), A self-regulating model of bedrock river channel geometry, *Geophys. Res. Lett.*, *33*, L04402, doi:10.1029/2005GL023193.

Stark, C. P., J. R. Barbour, Y. S. Hayakawa, T. Hattanji, N. Hovius, H. Chen, C.-W. Lin, M.-J. Horng, K.-Q. Xu, and Y. Fukahata (2010), The Climatic

Signature of Incised River Meanders, *Science*, *327*(5972), 1497–1501, doi:10.1126/science.1184406.

Stock, J. D., and D. R. Montgomery (1999), Geologic constraints on bedrock river incision using the stream power law, *J. Geophys. Res.*, *104*(B3), 4983–4993, doi:10.1029/98JB02139.

Tachikawa, T., et al. (2009), Advanced Spaceborne Thermal Emission and Reflection Radiometer (ASTER) Global Digital Elevation Model, edited by METI and NASA, Land Processes Distributed Active Archive Center (LP DAAC).

Thakur, V. C. (1995), Geology of Dun Valley, Garhwal Himalaya: Neotectonics and coeval deposition with fault-propogation folds, *J. Himalayan Geol.*, *6*(2), 1–8.

Thakur, V. C. (2013), Active tectonics of Himalayan Frontal Fault system, *Int J Earth Sci (Geol Rundsch)*, 1–20, doi:10.1007/s00531-013-0891-7.

Thakur, V. C., A. K. Pandey, and N. Suresh (2007), Late Quaternary–Holocene evolution of Dun structure and the Himalayan Frontal Fault zone of the Garhwal Sub-Himalaya, NW India, *J. Asian Earth Sci.*, *29*(2–3), 305–319, doi:10.1016/j.jseaes.2006.02.002.

Tomkin, J. H., M. T. Brandon, F. J. Pazzaglia, J. R. Barbour, and S. D. Willett (2003), Quantitative testing of bedrock incision models for the Clearwater River, NW Washington State, *J. Geophys. Res.*, *108*(B6), 2308, doi:10.1029/2001JB000862.

Turowski, J. M., D. Lague, and N. Hovius (2007), Cover effect in bedrock abrasion: A new derivation and its implications for the modeling of bedrock channel morphology, *J. Geophys. Res.*, *112*, F04006, doi:10.1029/2006JF000697.

Turowski, J. M., N. Hovius, H. Meng-Long, D. Lague, and C. Men-Chiang (2008), Distribution of erosion across bedrock channels, *Earth Surf. Processes and Landforms*, *33*, 353–363, doi:10.1002/esp.1559.

Walsh, L. S., A. J. Martin, T. P. Ojha, and T. Fedenczuk (2012), Correlations of fluvial knickzones with landslide dams, lithologic contacts, and faults in the southwestern Annapurna Range, central Nepalese Himalaya, *J. Geophys. Res.*, *117*, F01012, doi:10.1029/2011JF001984.

Wesnousky, S. G., S. Kumar, R. Mohindra, and V. C. Thakur (1999), Uplift and convergence along the Himalayan Frontal Thrust of India, *Tectonics*, *18*(6), 967–976, doi:10.1029/1999TC900026.

Whipple, K. X. (2004), Bedrock Rivers and the Geomorphology of Active Orogens, *Annu. Rev. Earth Planet. Sci.*, *32*(1), 151–185, doi:10.1146/annurev.earth.32.101802.120356.

Whipple, K. X., and G. E. Tucker (1999), Dynamics of the stream-power river incision model: Implications for height limits of mountain ranges, landscape response timescales, and research needs, *J. Geophys. Res.*, *104*(B8), 17,661–17,674, doi:10.1029/1999JB900120.

Whipple, K. X., G. S. Hancock, and R. S. Anderson (2000), River incision into bedrock: Mechanics and relative efficacy of plucking, abrasion, and cavitation, *Geol. Soc. Am. Bull.*, *112*(3), 490–503, doi:10.1130/0016-7606(2000)112<490:riibma>2.0.co;2.

Whittaker, A. C. (2012), How do landscapes record tectonics and climate?, *Lithosphere*, *4*(2), 160–164, doi:10.1130/rf.l003.1.

Whittaker, A. C., P. A. Cowie, M. L. Attal, G. E. Tucker, and G. P. Roberts (2007), Bedrock channel adjustment to tectonic forcing: Implications for predicting river incision rates, *Geology*, *35*(2), 103–106, doi:10.1130/g23106a.1.

Whittaker, A. C., M. Attal, P. A. Cowie, G. E. Tucker, and G. Roberts (2008), Decoding temporal and spatial patterns of fault uplift using transient river long profiles, *Geomorphology*, *100*(3–4), 506–526, doi:10.1016/j.geomorph.2008.01.018.

Wobus, C., K. X. Whipple, E. Kirby, N. Snyder, J. Johnson, K. Spyropolou, B. Crosby, and D. Sheehan (2006a), Tectonics from topography: Procedures, promise, and pitfalls, in *Geol. Soc. Spec. Pub.*, edited S. D. Willett, N. Hovius, M. T. Brandon, D. M. Fisher, pp. 55–74.

Wobus, C. W., G. E. Tucker, and R. S. Anderson (2006b), Self-formed bedrock channels, *Geophys. Res. Lett.*, *33*, L18408, doi:10.1029/2006GL027182.

Wobus, C. W., J. W. Kean, G. E. Tucker, and R. S. Anderson (2008), Modeling the evolution of channel shape: Balancing computational efficiency with hydraulic fidelity, *J. Geophys. Res.*, *113*, F02004, doi:10.1029/2007JF000914.

Wohl, E. (2004), Limits of downstream hydraulic geometry, *Geology*, *32*(10), 897–900, doi:10.1130/g20738.1.

Wohl, E., and G. C. L. David (2008), Consistency of scaling relations among bedrock and alluvial channels, *J. Geophys. Res.*, *113*, F04013, doi:10.1029/2008JF000989.

Wolman, M. G., and J. P. Miller (1960), Magnitude and frequency of forces in geomorphic processes, *J. Geol.*, *68*(1), 54–74, doi:10.1086/626637.

Yanites, B. J., and G. E. Tucker (2010), Controls and limits on bedrock channel geometry, *J. Geophys. Res.*, *115*, F04019, doi:10.1029/2009JF001601.

Yanites, B. J., G. E. Tucker, K. J. Mueller, Y.-G. Chen, T. Wilcox, S.-Y. Huang, and K.-W. Shi (2010), Incision and channel morphology across active structures along the Peikang River, central Taiwan: Implications for the importance of channel width, *Geol. Soc. Am. Bull.*, *122*(7–8), 1192–1208, doi:10.1130/b30035.1.

Yeats, R. S., and R. J. Lillie (1991), Contemporary tectonics of the Himalayan frontal fault system: folds, blind thrusts and the 1905 Kangra earthquake, *J. Struct. Geol.*, *13*(2), 215–225, doi:10.1016/0191-8141(91)90068-t.

Yeats, R. S., and V. C. Thakur (2008), Active faulting south of the Himalayan Front: Establishing a new plate boundary, *Tectonophysics*, *453*(1–4), 63–73, doi:10.1016/j.tecto.2007.06.017.